

Influences of various calculation options on heat, water and carbon fluxes determined by open- and closed-path eddy covariance methods

By MASAHITO UHEYAMA^{1*}, RYUICHI HIRATA², MASAYOSHI MANO³, KEN HAMOTANI¹, YOSHINOBU HARAZONO^{1,4}, TAKASHI HIRANO², AKIRA MIYATA³, KENTARO TAKAGI⁵ and YOSHIYUKI TAKAHASHI⁶, ¹Graduate School of Life and Environmental Sciences, Osaka Prefecture University, 1-1 Gakuen-cho, Naka-ku, Sakai, Japan; ²Research Faculty of Agriculture, Hokkaido University, Kita 9, Nishi 9, Kita-ku, Sapporo, Japan; ³National Institute for Agro-Environmental Sciences, 3-1-1 Kannondai, Tsukuba, Japan; ⁴International Arctic Research Center, University of Alaska Fairbanks, Fairbanks, Alaska, USA; ⁵Field Science Center for Northern Biosphere, Hokkaido University, Toikanbetu, Horonobe, Hokkaido, Japan; ⁶Center for Global Change Environmental Research, National Institute for Environmental Studies, 16-2 Onogawa, Tsukuba, Ibaraki, Japan

(Manuscript received 30 October 2011; in final form 7 June 2012)

ABSTRACT

Synthesis studies using multiple-site datasets for eddy covariance potentially contain uncertainties originating from the use of different flux calculation options, because the choice of the process for calculating half-hourly fluxes from raw time series data is left to individual researchers. In this study, we quantified the uncertainties associated with different flux calculation methods at seven sites. The differences in the half-hourly fluxes were small, generally of the order less than a few percentiles, but they were substantial for the annual fluxes. After the standardisation under current recommendations in the FLUXNET communities, we estimated the uncertainties in the annual fluxes associated with the flux calculations to be $2.6 \pm 2.7 \text{ W m}^{-2}$ (the mean 90% \pm confidence interval) for the sensible heat flux, $72 \pm 37 \text{ g C m}^{-2} \text{ yr}^{-1}$ for net ecosystem exchange (NEE), $12 \pm 6\%$ for evapotranspiration, $12 \pm 6\%$ for gross primary productivity and $16 \pm 10\%$ for ecosystem respiration. The self-heating correction strongly influenced the annual carbon balance ($143 \pm 93 \text{ g C m}^{-2} \text{ yr}^{-1}$), not only for cold sites but also for warm sites, but did not fully account for differences between the open- and closed-path systems ($413 \pm 189 \text{ g C m}^{-2} \text{ yr}^{-1}$).

Keywords: eddy covariance, flux calculation, multi-site analyses, systematic bias, uncertainties

1. Introduction

The eddy covariance method has been extensively used for understanding energy, water and carbon exchange in terrestrial ecosystems (e.g. Baldocchi et al., 2001; Baldocchi, 2003). This method provides continuous datasets at half-hourly to interannual time scales. In global and regional networks of eddy covariance measurements from various ecosystems (e.g. FLUXNET, AmeriFlux, CarboEurope-IP, AsiaFlux and CarboEastAsia), eddy covariance data have been used to understand the role of terrestrial ecosystems at

regional and global scales. Key applications include performing data comparisons among multiple sites (Valentini et al., 2000; Baldocchi et al., 2001; Baldocchi, 2008; Hirata et al., 2008; Beer et al., 2010) and model development, calibration and validation (Grant et al., 2005; Ito, 2008; Ueyama et al., 2010).

Although eddy covariance data have been widely used in synthesis studies, the following issues have been recognised: (1) standardised data processing is necessary (Papale et al., 2006; Mauder et al., 2008); (2) uncertainties in this method must be quantified (Goulden et al., 1996; Loescher et al., 2006; Mauder et al., 2008); and (3) these uncertainties must be reduced. Uncertainties have been associated with various factors, including random sampling errors (Richardson et al., 2006; Mano et al., 2007a), flux partitioning (Reichstein

*Corresponding author.
email: miyabi-flux@muh.biglobe.ne.jp

et al., 2005; Richardson and Hollinger, 2005; Lasslop et al., 2010), energy balance closure (Wilson et al., 2002; Mauder et al., 2010), the averaging interval (Sakai et al., 2001; Finnigan et al., 2003; Moncrieff et al., 2004; Mauder and Foken, 2006), gap-filling (Falge et al., 2001; Hirata et al., 2007; Moffat et al., 2007), processing of nocturnal data (Gu et al., 2005; Papale et al., 2006; Acevedo et al., 2009), discrepancies between open- and closed-path gas analyzers (Hirata et al., 2005; Burba et al., 2008; Haslwanter et al., 2009), the sonic anemometer angle of attack (Nakai et al., 2006), various instrumentation methods (Mauder et al., 2007; Nemitz et al., 2009) and sensor maintenance (Serrano-Ortiz et al., 2008). Recognising the need for standardised data processing, recent synthesis studies have used data that were reprocessed using standardised flux partitioning and gap-filling methods (e.g. Hirata et al., 2008; Grant et al., 2009); however, in most studies, flux calculations have been performed by researchers at individual sites (e.g. Luyssaert et al., 2007, 2008; Owen et al., 2007; Hirata et al., 2008). Although the current framework of FLUXNET establishes the standardisation of flux calculations (Aubinet et al., 2000; AsiaFlux 2007), the standardised calculation was not often applied partly owing to limited experiences in the eddy covariance method for individual researchers. In addition, the FLUXNET community has not yet arrived at a consensus (especially for newly proposed corrections) regarding the best way to calculate the flux with least uncertainties. Consequently, the flux calculated at each site may contain uncertainties due to inadequate calculations and corrections; synthesis studies that use the FLUXNET database (and other synthesis datasets) potentially contain uncertainties originating from the varieties of flux calculation methods employed. Those uncertainties will be in the database as long as individual researchers process raw data. Thus, the uncertainties associated with flux calculations should be quantified.

Many studies have been performed to quantify the uncertainties related to CO₂ flux calculations. Goulden et al. (1996) quantified the uncertainty associated with sampling error as 30 g C m⁻² yr⁻¹ using a single year of data at a forest site. Mano et al. (2007a) reported that the effect of the random sampling error was less than 2% of the annual carbon flux at a rice paddy site. Takagi et al. (2008) compared carbon fluxes at a forest site calculated using different types of eddy-flux software and found that the uncertainty associated with the systematic error was less than 150 g C m⁻² yr⁻¹. Only a few analyses of uncertainty have been conducted using a multisite dataset. Mauder et al. (2008) compared half-hourly CO₂ fluxes derived using different eddy covariance software platforms for data collected from four sites of the CarboEurope-IP network and found that the differences were within 5–10% on a half-hourly time scale. The authors suggested that the

uncertainties were caused mainly by the spike detection algorithm, lag-time correction, coordinate rotation and high-frequency loss correction. However, because they compared the fluxes calculated using existing eddy covariance software packages, they could not completely isolate the effects of individual data processing steps. Thus, it is still unclear which data processing steps are influential in the calculation of half-hourly and annual fluxes. Studies that apply well-designed sets of data processing methods to multisite data are required to identify uncertainties associated with flux calculations.

In this study, we quantified the uncertainties associated with flux calculations in half-hourly and annual fluxes measured by both open- and closed-path systems. We used 1-year raw datasets from seven flux sites with a variety of vegetation types, ranging from Arctic tundra to tropical forest. To efficiently process datasets from seven sites by applying various sets of flux calculation options, we developed new eddy covariance software. We also evaluated differences in the fluxes produced by open- and closed-path systems. This is important because multisite datasets used in synthesis studies often include fluxes measured by an open-path system together with those measured by a closed-path system.

2. Measurements

In this study, we used eddy covariance data from seven sites, covering a range of climates from the Arctic to the tropics, and a range of plant functional types, including tundra, agricultural fields, and deciduous and evergreen forests (Fig. 1, Table 1).

BRW is an Arctic tundra site in Barrow, Alaska, USA (Harazono et al., 2003) with a flat terrain. The vegetation at this site consists of wet sedges, grasses, mosses and lichens, and the dominant species is *Arctophila fulva*. The vegetation is completely flooded after snow melt. The 2003 growing season began in mid-June, and senescence occurred at the end of mid-September. An open-path eddy covariance system was installed at a height of 1.9 m.

UAF is a boreal black spruce (*Picea mariana*) forest in Fairbanks, Alaska, USA (Ueyama et al., 2006). The forest consists of an open canopy with understory vegetation, and the forest floor is completely covered by mosses and lichens. The climate is continental with calm wind conditions. The 2007 growing season began in late April and ended in late September. An open-path eddy covariance system was installed at a height of 6 m. The CO₂ concentration profile was measured with an infrared gas analyzer (IRGA) (LI840, Li-Cor, USA) at 4 heights.

TSE is a young hybrid larch (*Larix gmelinii* × *Larix kaempferi*) forest with dense undergrowth (*Sasa senanensis* and *Sasa kurilensis*) in the Teshio Experimental Forest of

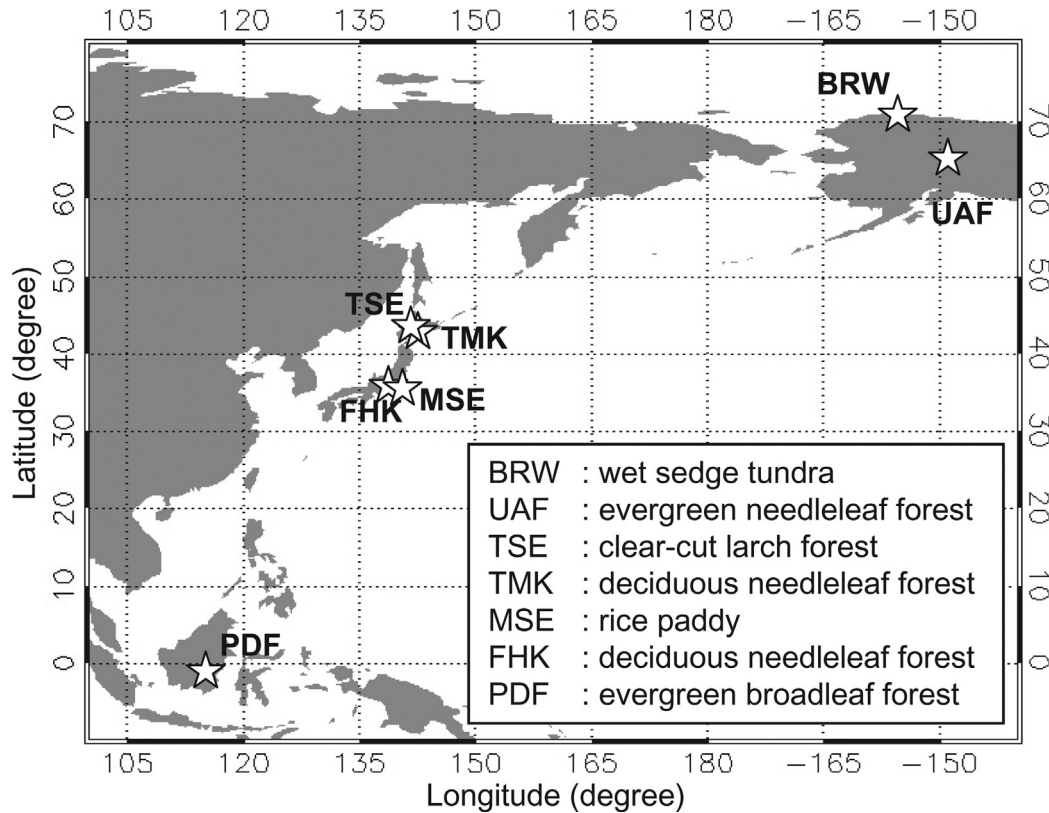


Fig. 1. Locations and vegetation types of the study sites.

Hokkaido University, Japan (Takagi et al., 2009). The mixed forest was cut from January to March 2003, and then the hybrid larch were planted on a flat terrain. The dominant vegetations consisted of the hybrid larch, *S. senanensis* and *S. kurilensis*. Open- and closed-path eddy covariance systems were installed at a height of 5.7 m. The CO₂ concentration profile was measured at 4 (snow-covered period) or 5 (snow-free period) heights with an IRGA (DX6100; RMT Ltd., Russia).

TMK is a planted Japanese larch (*L. kaempferi*) forest located approximately 15 km northwest of Tomakomai, Hokkaido, in Northern Japan (Hirano et al., 2003; Hirata et al., 2007). The terrain is nearly flat with a slope of 1–2°, and the canopy is homogeneous. Latent heat and CO₂ fluxes were measured with both open- and closed-path systems. CO₂ concentration profile was measured by an IRGA (LI6262, Li-Cor) at 10 heights.

MSE is an artificially irrigated rice paddy in Mase, Japan (Saito et al., 2005; Mano et al., 2007a) on a uniformly flat area. The paddy fields at this site were managed as single rice crop fields; in 2005, rice (*Oryza sativa*) was transplanted on May 2 and harvested on September 13. A closed-path eddy covariance system was only employed from April 15 to October 21, whereas an open-path system was operated throughout the year. The measurement

height was changed from 3.0 to 3.3 m considering the growth stage. CO₂ concentration profile was measured by an IRGA (LI7000, Li-Cor) at 5 heights.

FHK is a planted Japanese larch (*L. kaempferi*) forest located in Fujiyoshida, Japan (Ueyama et al., 2012). The terrain at this site has a slope of 3–4°, and the canopy is homogeneous. Fluxes were measured with both open- and closed-path systems installed at 35 m, and CO₂ concentration profile was measured by an IRGA (LI6262, Li-Cor) at 10 heights.

PDF is a tropical peat swamp forest located near Palangkaraya, Central Kalimantan province, Indonesia (Hirano et al., 2007). This site consists of a homogeneous secondary forest with a flat terrain. The dominant species are *Combretocarpus rotundatus*, *Cratoxylum arborescens*, *Buchanania sessifolia* and *Tetramerista glabra*. An open-path eddy covariance system was installed at a height of 41 m. CO₂ concentration profile was measured by an IRGA (LI820, Li-Cor) at 6 heights.

3. Data processing

To quantify the uncertainties associated with flux calculation options, we examined half-hourly and annual values for sensible heat, water vapor and CO₂ fluxes. With the

Table 1. Annual values of fluxes and the u^* -threshold of the control calculation. The differences between the open- and closed-path systems are also shown

Site	Climate	Vegetation	Location	Year	Canopy height (m)	T_{annual} ($^{\circ}\text{C}$)
BRW	Arctic	Wet sedge tundra	71°19'13"N, 156°37'20"W	2003	0.1	−11.5
UAF	Boreal	Black spruce forest	64°52'N, 147°51'W	2007	1.5	−3.5
TSE	Temperate	Larch and <i>Sasa</i> forest	45°03'N, 142°06'E	2010	1.5 (<i>Sasa</i>)–3 (larch)	6.5
TMK	Temperate	Larch forest	42°44'N, 141°31'E	2003	15	6.6
MSE	Temperate	Rice paddy	36°3'N, 140°01'E	2005	0.05–1.2	13.3
FHK	Temperate	Larch forest	35°26'38"N, 138°45'53"E	2006	17	9.6
PDF	Tropical	Peat swamp forest	2°20'42"S, 114°2'11"E	2003–2004	26	26.1

Site	Measurement height (m)	Sampling (Hz)	Sonic anemometer model	IRGA model	Sonic span (m)	Sensor separation (m)
BRW	1.9	10	DA600-TR62AX ^a	LI7500 ^c	0.1	0.15
UAF	6	10	CSAT3 ^b	LI7500 ^c	0.1	0.30
TSE	5.6	10	DA600-3TV ^a	LI7500 ^c /LI7000 ^c	0.2	0.38
TMK	27	10	DA600-3TV ^a	LI7500 ^c /LI6262 ^c	0.2	0.49
MSE	3.0–3.3	10	DA600-TR62AX ^a	LI7500 ^c /LI7000 ^c	0.1	0.25
FHK	35	10	DA600-3TV ^a	LI7500 ^c /LI6262 ^c	0.2	0.30
PDF	41	10	CSAT3 ^b	LI7500 ^c	0.1	0.20

^aKaijo, Japan.

^bCampbell Scientific Inc., USA.

^cLi-Cor, USA.

Note: T_{annual} is mean annual air temperature.

exception of the flux calculations, we performed standardised data processing steps that included quality control (QC), friction velocity (u^*)-filtering and gap-filling (Fig. 2). The details of each processing step are described in later subsections and appendices. To apply the data processing steps, we developed an eddy covariance software (referred to as the Flux Calculator program). This software calculates eddy fluxes, turbulence statistics, spectral characteristics, QC information and flux footprints, and it includes the options necessary to process eddy covariance data, such as coordinate rotation, detrending, crosswind correction, lag-time correction, high-frequency loss correction and correction for the self-heating effect of an open-path sensor. Another software platform (the Flux Analysis Tool program) performs u^* -threshold determination, gap-filling and flux partitioning calculations. We calculated half-hourly eddy fluxes from 10-Hz raw data using this software with different calculation options and then compared the results on a half-hourly and an annual basis. The experimental design is shown in Table 2.

3.1. Flux calculations and software

In this study, we calculated fluxes with and without various calculation options. The flow of the flux calculations is shown in Fig. 3. Before performing flux calculations, a spike detection algorithm was implemented; fluctuations that deviated by more than five standard deviations from

mean of 5-min block sub-windows were removed from the raw data and the rejected data were eliminated from subsequent processing. The flux was calculated as the 30-min covariance of the vertical wind velocity and a scalar quantity (CO_2 , water vapor and air temperature). The software has first- and second-order detrending options. The coordinate rotation (tilt correction) of sonic anemometers was chosen from four options: double, extended double, triple and planar fit rotations (Wilczak et al., 2001). Under double rotation, the tilt angle was determined for individual half-hourly data, whereas for extended double rotation, the tilt angle was determined for 360 wind sectors using the whole (1-year) dataset. For the MSE site, the tilt angle for extended double rotation and parameters for planar fit rotation were determined for each management period: before transplanting, from transplanting to harvesting and after harvesting. In the triple rotation (TR), a third rotation of sonic anemometer wind components is applied according to McMillen (1988). The software corrected artificial fluctuations in the virtual air temperature caused by crosswind (Kaimal and Gaynor, 1991) and water vapor (Hignett, 1992); the crosswind correction was not applied when the correction was internally processed by the sonic anemometer (e.g. CSAT3, Campbell Scientific, Inc., USA). Correction for high- and low-frequency losses was performed using a theoretical transfer function for fluxes of momentum, sensible heat and $\text{CO}_2/\text{H}_2\text{O}$ by open-path system (Massman, 2000, 2001), which included effects of

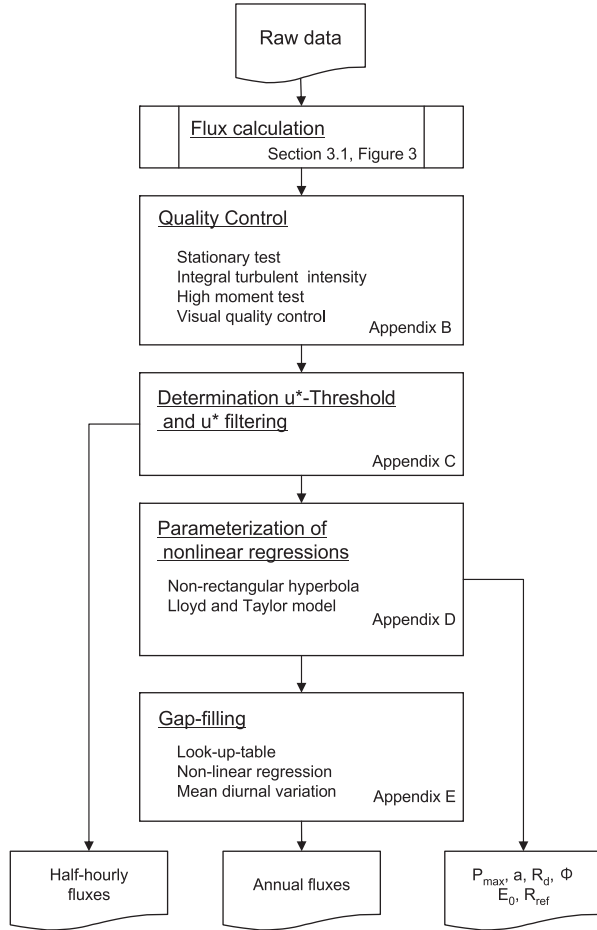


Fig. 2. Schematic of the processing of half-hourly and annual fluxes as well as related parameters for non-linear regressions. In this study, all of the processing steps except flux calculation were conducted in the same manner. The details of the flux calculations are shown in Fig. 3.

line averaging, sensor separation and high-pass filtering due to block averaging and linear detrending. The high-frequency loss associated with sensor separation was theoretically corrected by considering wind direction. Instead of employing methods by Massman, the high-frequency loss was corrected via empirical functions (Appendix A; Aubinet et al., 2000) for CO₂ and H₂O fluxes by closed-path systems; the cutoff frequency was empirically determined for each site by considering the cospectra of sensible heat flux and CO₂ and H₂O fluxes obtained from closed-path sensor. The effect of relative humidity to cutoff frequency of closed-path system (Ibrom et al., 2007) was corrected according to Mammarella et al. (2009) (Appendix A; hereafter, we refer as the Mammarella correction). The software corrected for the lag-time of the signals between the anemometer and the closed-path sensor using a cross correlation. The prescribed lag-time between

sonic anemometer and open-path sensor was corrected; for example, lag-time between DA600 (Kaijo, Japan) and LI7500 (Li-Cor) is 0.1 s and between CSAT3 (Campbell Scientific Inc., USA) and LI7500 (Li-Cor) is 0.0 s. After performing the flux calculations, the WPL correction was applied to compensate for density fluctuations (Webb et al., 1980). The self-heating effect caused by the open-path sensor (LI7500, Li-Cor) was corrected according to Burba et al. (2008) and Amiro (2010); the effect was estimated from the air temperature, solar radiation and wind speed for the daytime and from the air temperature, downward long-wave radiation and wind speed for the nighttime. The CO₂/H₂O signals from closed-path sensor are corrected for a dilution effect by water vapor if closed-path sensor did not perform the correction internally; there is an option to perform this correction in LI6262 (Li-Cor) but not in LI7000 (Li-Cor).

The CO₂ storage term for UAF, TSE, TMK, MSE, FHK and PDF was calculated based on CO₂ concentration at several measurement heights. For the BRW site, storage term was calculated from signal from the open-path sensor even though the storage term could be negligible considering the short canopy height (0.1 m) and the windy conditions.

3.2. Experimental design

In this study, we quantified the uncertainties in the sensible heat, water vapor and CO₂ fluxes associated with various calculation options using data from seven sites. We calculated these fluxes according to the experimental design shown in Table 2. As a control experiment, we calculated the half-hourly fluxes by applying all preferable corrections (AsiaFlux, 2007). The applied corrections were the despiking, the crosswind and water vapor corrections to the sensible heat flux, double rotation, the high-frequency loss correction, the prescribed lag-time correction between open-path sensor and sonic anemometer and the lag-time correction for the closed-path systems (Table 2; Fig. 3). To understand how the choice of a single calculation option affects the half-hourly fluxes, we calculated fluxes by changing sets of calculation options (from NoDR to Storage in Table 2). The no-crosswind correction experiment (NoCW) was conducted only for the sites where sonic anemometers other than CSAT3 were used because CSAT3 automatically corrects for the effect of crosswind in its firmware.

Furthermore, to quantify how the difference in the half-hourly fluxes associated with different calculation options was propagated to the annual fluxes through the data survival rate, the u^* -threshold and gap-filling, we applied a standardised data processing method to each calculated half-hourly flux dataset in a consistent fashion. The applied

Table 2. In the control experiment, the flux calculation was performed by applying all preferable corrections: the despiking, the crosswind and water vapor corrections to the sensible heat flux, the double rotation, the high-frequency loss correction, the prescribed lag-time correction between open-path sensor and sonic anemometer, a lag-time correction for the closed-path systems and the WPL correction

Experiment	Despiking	Detrending	Rotation	Crosswind ^a	Water vapor	Lag-time open	Lag-time closed	High-frequency loss	Mammarella	WPL	SelfHeat ^b	Storage
Control	○		○	○	○	○	○	○		○		
NoDR	○			○	○	○	○	○		○		
PFR ^c	○		○	○	○	○	○	○		○		
DRExt ^d	○		○	○	○	○	○	○		○		
TR ^e	○		○	○	○	○	○	○		○		
NoWV	○		○	○		○	○	○		○		
NoCW	○		○		○	○	○	○		○		
NoDespike			○	○	○	○	○	○		○		
Detrend1 ^f	○	○	○	○	○	○	○	○		○		
Detrend2 ^g	○	○		○	○	○	○	○		○		
NoHL	○		○	○	○	○	○			○		
SelfHeat	○		○	○	○	○	○	○		○	○	
Mammarella	○		○	○	○	○	○		○	○		
Storage	○		○	○	○	○	○	○		○		○

^aA no crosswind correction experiment (NoCW) was conducted only for sites where CSAT3 was not used because CSAT3 automatically corrected the effect of crosswind to the virtual air temperature.

^bThe self-heating correction was only for the open-path eddy covariance systems.

^cIn PFR experiment, a planar fit rotation is applied.

^dIn DRExt experiment, an extended double rotation is applied.

^eIn TR experiment, a triple rotation is applied.

^fIn Detrend1 experiment, a first-order detrending is applied.

^gIn Detrend2 experiment, a second-order detrending is applied.

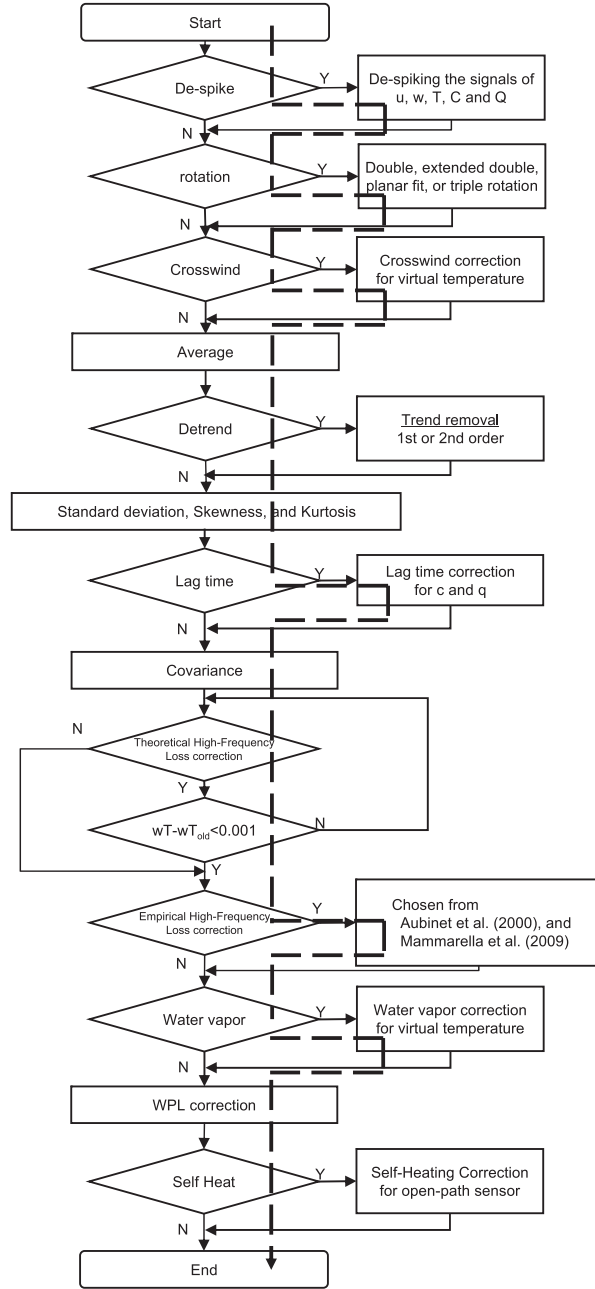


Fig. 3. Flowchart of the flux calculation. Theoretical high-frequency loss corrections are applied to momentum, heat and CO₂/H₂O fluxes by open-path systems, whereas empirical ones are for CO₂/H₂O fluxes by closed-path systems. The dashed line represents the flow of the control calculation. In the control calculation, double rotation is applied for the coordinate rotation, and the empirical high-frequency loss correction by Aubinet et al. (2000) is applied to closed-path systems.

standardised method encompassed quality control (Appendix B), the u^* -filtering correction (Appendix C), flux partitioning (Appendix D) and gap-filling (Appendix E).

The non-rectangular hyperbola and Lloyd and Taylor models (e.g. Lloyd and Taylor, 1994; Reichstein et al., 2005) were used for flux partitioning and gap filling. To exclude further uncertainties not related to the flux calculation options, we did not apply the storage correction in the control calculation, but influence of the storage correction was examined in a comparative calculation. For the sites where both open- and closed-path systems were employed (sites TSE, TMK, FHK and MSE), we calculated the fluxes for both systems. After all of these calculation and processing steps, we compared the half-hourly and annual fluxes corrected using various sets of flux calculation options with those obtained using the control calculation.

3.3. Quantification of uncertainties

We considered the uncertainties associated with the different calculation options only in terms of the range of potential variation of fluxes by taking the different calculation options, for the following reasons: (1) there is no single flux calculation method applicable to all sites with least uncertainties; and (2) flux data that were inadequately calculated may be present in current databases by FLUX-NET and other synthesis studies. Thus, the uncertainties used in this study represent the uncertainty potentially exist in the multisite database rather than that related to individual flux measurements. For individual measurements, the uncertainties defined here are solely the differences associated with the calculation options.

We quantified the uncertainties as the slope and intercept values between the control and comparative fluxes from a regression analysis on a half-hourly basis. The slope and intercept measures systematic biases on average: the slope represents a bias in proportion to flux magnitude, and the intercept represents a constant bias on all the flux range.

The annual uncertainties in each site were quantified from the difference between the control and comparative calculations (control calculation minus comparative calculation) in the annual values for the sensible heat and CO₂ fluxes. Because the annual differences for evapotranspiration (ET), gross primary productivity (GPP) and ecosystem respiration (RE) were dependent on their absolute values, we quantified the uncertainties for the annual ET, GPP and RE from the ratio of the fluxes by the comparative calculation via the control calculation rather than the difference. To avoid any ambiguity between the differences and ratios, the annual values calculated by the control calculation are shown in Table 3; this enabled us to translate from the differences to the ratios and vice versa. The systematic biases in the half-hourly fluxes caused by the different calculation options propagate to the annual fluxes through the post-processing procedures

Table 3. Annual values of fluxes and the u^* -threshold of the control calculation. The differences between the open- and closed-path systems are also shown

Site	System	H (W m^{-2})	ET (mm yr^{-1})	Difference ET ^a (mm yr^{-1})	NEE ($\text{g C m}^{-2} \text{ yr}^{-1}$)	Difference NEE ^a ($\text{g C m}^{-2} \text{ yr}^{-1}$)	GPP ($\text{g C m}^{-2} \text{ yr}^{-1}$)	Difference GPP ^a ($\text{g C m}^{-2} \text{ yr}^{-1}$)	RE ($\text{g C m}^{-2} \text{ yr}^{-1}$)	Difference RE ^a ($\text{g C m}^{-2} \text{ yr}^{-1}$)	u^* -threshold (m s^{-1})
BRW	Open	5.1	132		-169		252		83		0.23
UAF	Open	11.3	239		6		721		727		0.18
TSE	Open	-2.2	409	124	-322	-407	1429	25	1107	-382	0.25
	Closed		285		85		1404		1488		0.28
TMK	Open	24.9	637	163	-657	-453	1993	-99	1337	-552	0.34
	Closed		474		-204		2092		1888		0.35
FHK	Open	33.7	504	29	-895	-591	2113	225	1218	-366	0.33
	Closed		475		-304		1888		1584		0.30
MSE	Open	-0.5	956	178	-246	-203	1170	-22	924	-225	0.20
	Closed ^b		382		-166		1124		958		0.19
PDF	Open	20.3	1282		53		3198		3251		0.24

^aThe difference is calculated as flux by the closed-path system subtracted from the open-path system.^bThe closed path system in the MSE site were only operated in the growing season between DOY 105 and 294. The difference between the open- and closed-path systems were calculated for this period.

(quality control, gap-filling and u^* -filtering). Although the standardised post-processing procedure was applied to all the sites in this study, the propagation of the systematic biases in half-hourly fluxes to the annual fluxes changes with site conditions. As the annual uncertainties for individual site is taken as 90% confidence interval for the t -distribution considering the range of the annual fluxes by different calculations. The defined annual uncertainty for individual site represents that 90% of variations in the annual fluxes are fallen in this range owing to the various calculation options and includes not only the direct effect of the biases in half-hourly fluxes by the different calculation options but also their indirect effects propagated through the post-processing procedures.

The annual uncertainties in multisite data were calculated as the mean of the annual uncertainties in individual site, representing the range of variation associated from various flux calculation options. We quantified this annual uncertainties from two datasets: (1) fluxes calculated in case all the processing was arbitrarily chosen (potential range of uncertainties) and (2) standardised fluxes calculated by including the recommended processing (range of uncertainties in data processed by the standardised methodology). We refer to significant bias in the annual basis when mean of comparative annual fluxes at each site significantly differed from that by the control calculation ($p < 0.1$).

4. Results

4.1. Half-hourly time scale

First, we compared the half-hourly fluxes calculated in the control experiment with those applied using various sets of flux calculation options. A scatter diagram was constructed for the half-hourly fluxes obtained by the control experiment (x -axis) and those produced by the other experiments shown in Table 2 (y -axis), and the slopes and intercepts of the scatter plot were then determined using regression analysis. The slopes and intercepts for the sensible heat (H), latent heat (LE) and CO_2 (Fc) fluxes are shown in Fig. 4 for the open-path systems and in Fig. 5 for the closed-path systems. Those values were also shown in Tables 4 and 5.

The slope values between the double rotation (control) and other rotation options ranged from +3% to -11% (Figs. 4 and 5, and Table 4). The slopes for TR significantly deviated further from 1.0 than the other rotational options (Figs. 4 and 5; Table 4). The average determination coefficient (R^2) between the control and TR calculations were 0.95 for all H, LE and Fc. These R^2 values were substantially lower than the R^2 between the control and the other rotation options (more than 0.99). The lower R^2 values in TR indicated that application of TR amplified the random error.

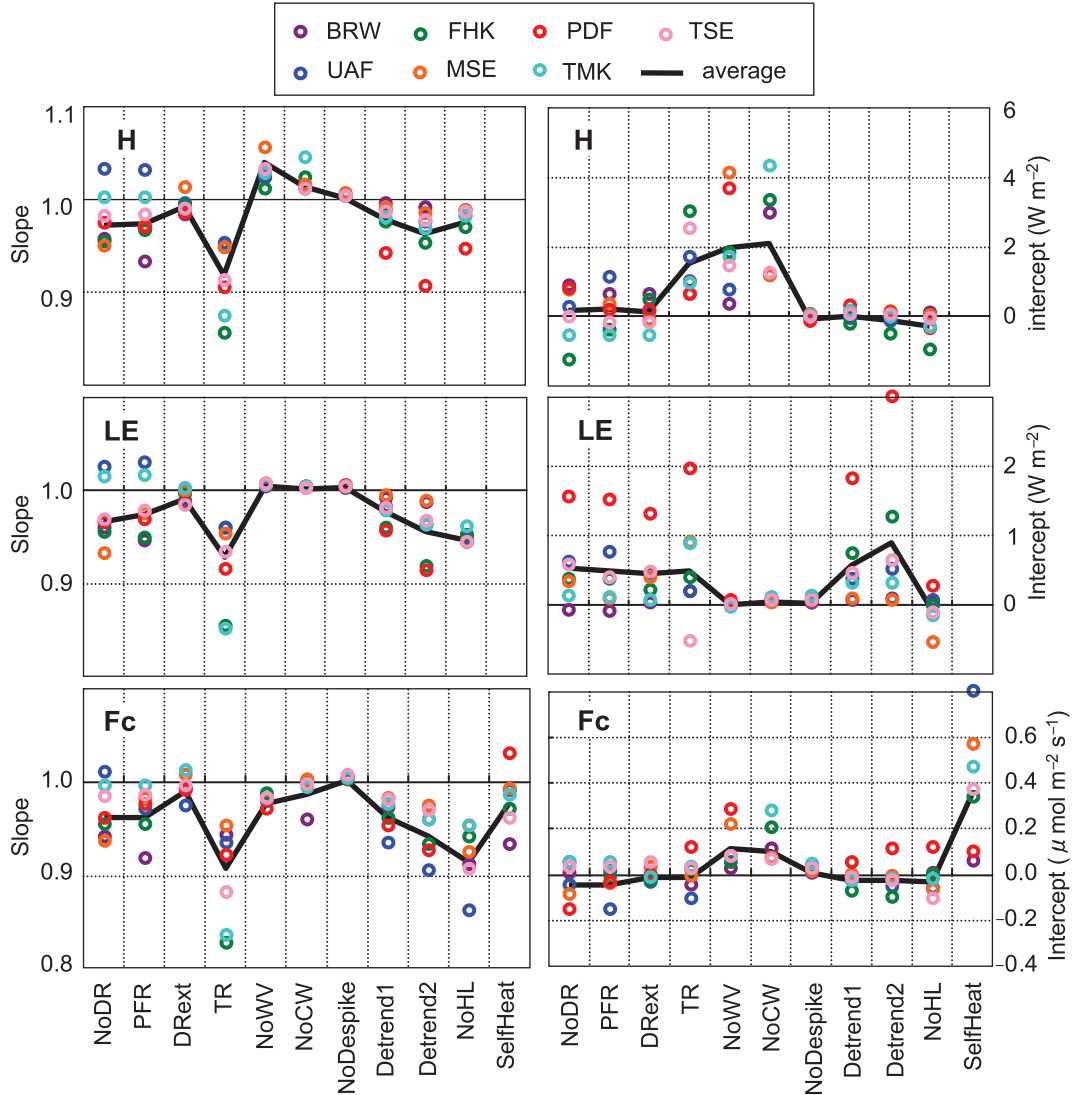


Fig. 4. Slope and intercept determined by regression of the half-hourly fluxes between the control and comparative calculations for the open-path systems. The following corrections were applied: no double rotation (NoDR), planar fit rotation (PFR), extended DR (DRext), triple rotation (TR), no water vapor correction (NoWV), no crosswind correction (NoCW), no despiking (NoDespike), first-order detrending (Detrend1), second-order detrending (Detrend2), no high-frequency loss correction (NoHL) and self-heating correction (SelfHeat).

The no water vapor correction for the sonic virtual temperature significantly increased H in both the slope and intercept values (Tables 4 and 5). The greater slope values and positive intercept values propagated to Fc through the WPL correction and then decreased in CO₂ uptake measured by open-path systems (-2% in the slope values; $p < 0.05$) were examined (Fig. 4). The effect was most remarkable in humid sites in tropical rainforest (PDF) and rice paddy (MSE). The no-crosswind correction weakly increased the H (Tables 4 and 5) and propagated to Fc (decrease of uptake through increase in the intercept) through the WPL correction (Fig. 4 and Table 5).

Despiking did not strongly influence the half-hourly fluxes. The slopes and intercepts were close to 1.0 and 0.0, respectively, for all of the fluxes and sites. Detrending preprocessing significantly reduced the calculated fluxes by up to 10% (Fig. 4; Table 4).

The high-frequency loss correction was also substantial at the sites where the closed-path system was used (26% for LE and 13% for Fc; $p < 0.01$) (Fig. 5 and Table 4); where the daytime flux (26% for LE and 11% for Fc; $p < 0.01$) and nighttime flux (49% for LE and 25% for Fc; $p < 0.01$) were corrected on average. Similar to closed-path fluxes, the effect of the high-frequency loss correction for the

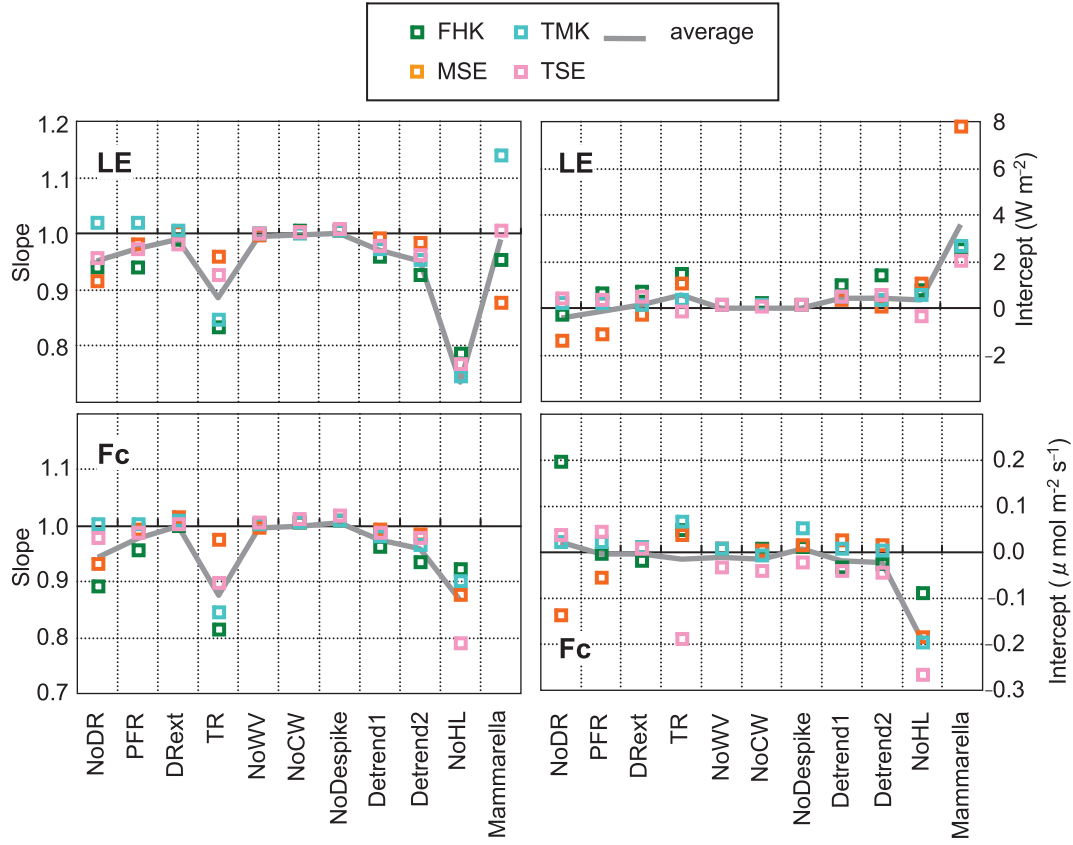


Fig. 5. Slope and intercept determined by regression of the half-hourly fluxes between the control and comparative calculations for the closed-path systems. In the closed-path calculation, the relative humidity effect for the high-frequency loss correction (Mammarella correction) was examined.

open-path systems was generally greater at night (6% for LE and 9% for Fc) than during the day (5% for LE and 7% for Fc). Because LE and Fc measured by open-path systems were corrected by same transfer function, the effects by high-frequency loss correction must be theoretically same for LE and Fc. The examined difference in the slope values for LE and Fc was caused by difference in the survived data after the quality control and difference in magnitude of the fluxes before corrected the high-frequency loss.

For the control calculation, half-hourly fluxes of LE and Fc by the open- and closed-path methods were consistent; the slope (x -axis is the open-path and y -axis is the closed-path fluxes) is 0.99 ± 0.06 for LE and 1.00 ± 0.06 for Fc (Table 6), whereas the intercept values were $-6 \pm 11 \text{ W m}^{-2}$ for LE and $0.98 \pm 0.28 \text{ } \mu\text{mol m}^{-2} \text{ s}^{-1}$ for Fc.

Influence of the relative humidity correction (the Mammarella correction; Mammarella et al., 2009) were different in each site in terms of slope value for LE by the closed-path, but the correction significantly increased intercept values ($p < 0.08$) (Fig. 5). The increase in the intercept showed that this correction effectively increased

smaller LE at nighttime when relative humidity was higher. By applying the Mammarella correction, correlation between LE by open- and closed-path systems did not significantly increase (Table 6), because the correlation was already high even when the correction was not applied.

The open-path self-heating correction on Fc significantly increased the intercept values ($0.38 \text{ } \mu\text{mol m}^{-2} \text{ s}^{-1}$; $p < 0.05$) (Fig. 4 and Table 5). The larger intercept of $0.52 \text{ } \mu\text{mol m}^{-2} \text{ s}^{-1}$ was in daytime than in nighttime ($0.25 \text{ } \mu\text{mol m}^{-2} \text{ s}^{-1}$). The intercepts from other calculation options were smaller than these values (Fig. 4). This indicates that the self-heating correction strongly decreased the sink of CO_2 at a half-hourly time scale. The intercept value was great in the calm site of UAF and least in the windy site of BRW.

4.2. Annual time scale

The annual uncertainties in the rotation options among double, extended double and planar fit rotation were 3.8 W m^{-2} for H, 6% for ET, $78 \text{ g C m}^{-2} \text{ yr}^{-1}$ for net ecosystem exchange (NEE) produced by the open-path systems and

Table 4. Slope values of linear regression between control and other experiments at a half-hourly basis. Slopes greater than 1 represent that fluxes from comparative experiments had greater magnitude than those from the control experiment

Flux	Site	System	NoDR	PFR	DRext	TR	NoWV	NoCW	NoDespike	Detrend1	Detrend2	NoHL	SelfHeat	Mammarella
H	BRW		0.96	0.93	0.98	0.95	1.02	1.01	1.00	0.99	0.99	0.99	—	—
	UAF		1.03	1.03	0.99	0.95	1.02	—	1.00	0.99	0.97	0.98	—	—
	TSE		0.98	0.98	0.99	0.91	1.03	1.01	1.00	0.98	0.98	0.98	—	—
	TMK		1.00	1.00	1.00	0.87	1.03	1.04	1.00	0.98	0.97	0.98	—	—
	FHK		0.95	0.96	0.99	0.85	1.01	1.02	1.00	0.97	0.95	0.97	—	—
	MSE		0.95	0.97	1.01	0.95	1.05	1.01	1.00	0.99	0.98	0.99	—	—
	PDF		0.97	0.97	0.98	0.90	1.10	—	1.00	0.94	0.91	0.95	—	—
	Average ^a		0.98 ^{ns}	0.98 ^{ns}	0.99 ^{ns}	0.99*	1.04**	1.02**	1.00**	0.98**	0.96*	0.98*	—	—
LE	BRW	Open	0.96	0.94	1.00	0.96	1.00	1.00	1.00	0.99	0.99	0.95	—	—
	UAF	Open	1.02	1.03	0.99	0.96	1.00	—	1.00	0.98	0.96	0.94	—	—
	TSE	Open	0.97	0.98	0.98	0.93	1.00	1.00	1.00	0.98	0.96	0.94	—	—
		Closed	0.95	0.97	0.98	0.92	0.99	1.00	1.00	0.97	0.96	0.76	—	1.00
	TMK	Open	1.01	1.01	1.00	0.85	1.00	1.00	1.00	0.98	0.96	0.96	—	—
		Closed	1.01	1.01	1.00	0.84	1.00	1.00	1.00	0.97	0.95	0.74	—	1.13
	FHK	Open	0.95	0.95	0.99	0.85	1.00	1.00	1.00	0.96	0.92	0.95	—	—
		Closed	0.94	0.94	0.99	0.83	1.00	1.00	1.00	0.95	0.92	0.78	—	0.95
	MSE	Open	0.93	0.97	1.00	0.95	1.00	1.00	1.00	0.99	0.99	0.94	—	—
		Closed	0.91	0.97	1.00	0.95	0.99	1.00	1.00	0.99	0.98	0.66	—	0.87
	PDF	Open	0.96	0.97	0.98	0.91	1.01	—	1.00	0.95	0.91	0.94	—	—
	Average ^a	Open	0.97 ^{ns}	0.98 ^{ns}	0.99**	0.92*	1.00*	0.83*	1.00*	0.98*	0.96*	0.95*	—	—
		Closed	0.95 ^{ns}	0.97 ^{ns}	0.99 ^{ns}	0.89*	0.99*	1.00 ^{ns}	1.00*	0.97*	0.95*	0.74*	—	0.99 ^{ns}
		Both	0.97**	0.98 ^{ns}	0.99**	0.91*	1.00 ^{ns}	1.00 ^{ns}	1.00*	0.97*	0.95*	0.87*	—	0.99 ^{ns}
Fc	BRW	Open	0.94	0.92	0.99	0.94	0.98	0.96	1.00	0.97	0.96	0.91	—	—
	UAF	Open	1.01	0.97	0.97	0.93	0.98	—	1.00	0.93	0.90	0.86	0.99	—
	TSE	Open	0.98	0.98	0.99	0.88	0.98	1.00	1.00	0.98	0.97	0.91	0.96	—
		Closed	0.97	0.98	1.00	0.89	1.00	1.00	1.01	0.98	0.97	0.78	—	1.00
	TMK	Open	0.99	0.99	1.00	0.83	0.98	0.99	1.00	0.97	0.96	0.95	0.98	—
		Closed	1.00	1.00	1.00	0.84	0.99	1.00	1.00	0.98	0.96	0.89	—	1.00
	FHK	Open	0.95	0.95	0.99	0.82	0.99	1.00	1.00	0.96	0.93	0.94	0.97	—
		Closed	0.89	0.95	0.99	0.81	1.00	1.00	1.00	0.96	0.93	0.92	—	0.94
	MSE	Open	0.93	0.98	1.00	0.95	0.98	1.00	1.00	0.98	0.97	0.92	0.99	—
		Closed	0.93	0.99	1.01	0.97	0.99	1.00	1.00	0.99	0.98	0.87	—	1.00
	PDF	Open	0.96	0.97	0.99	0.92	0.97	—	1.00	0.95	0.92	0.95	1.03	—
	Average ^a	Open	0.97**	0.97*	0.99 ^{ns}	0.90*	0.98*	0.99 ^{ns}	1.00*	0.96*	0.94*	0.92*	0.99 ^{ns}	—
		Closed	0.95 ^{ns}	0.98 ^{ns}	1.00 ^{ns}	0.88*	1.00**	1.00 ^{ns}	1.00 ^{ns}	0.98*	0.96*	0.87*	—	0.99 ^{ns}
		Both	0.96*	0.97*	0.99 ^{ns}	0.89*	0.98*	0.99 ^{ns}	1.00**	0.97*	0.95*	0.90*	0.99 ^{ns}	0.99 ^{ns}

^aSuperscripts of “ns”, “*”, and “**” represent that averaged slope was statistically no significant from 1.0 ($p > 0.10$), significant ($p < 0.05$), and significant ($0.05 < p < 0.10$), respectively.

Table 5. Intercept values of linear regression between control and other experiments at a half-hourly basis. Positive values represent that fluxes from comparative experiments were larger than those from the control experiment

Flux	Site	System	NoDR	PFR	DRext	TR	NoWV	NoCW	NoDespike	Detrend1	Detrend2	NoHL	SelfHeat	Mammarella
H (W m ⁻²)	BRW		0.81	0.58	0.58	0.96	0.31	2.91	-0.01	-0.04	-0.07	0.03	-	-
	UAF		0.21	1.08	0.10	1.65	0.70	-	-0.08	-0.11	-0.20	-0.07	-	-
	TSE		-0.09	-0.25	-0.25	2.47	1.40	1.20	-0.07	0.02	0.00	-0.12	-	-
	TMK		-0.61	-0.62	0.05	0.92	1.64	4.27	-0.04	0.08	-0.06	-0.34	-	-
	FHK		-1.29	-0.43	0.42	2.97	1.76	3.28	-0.03	-0.26	-0.57	-1.04	-	-
	MSE		0.70	0.28	-0.17	0.57	4.08	1.10	-0.01	0.09	0.10	-0.01	-	-
	PDF		0.75	0.11	0.14	0.59	3.63	-	-0.18	0.27	0.06	-0.41	-	-
	Average		0.07 ^{ns}	0.11 ^{ns}	0.12 ^{ns}	1.45**	1.93**	2.55**	-0.06 ^{ns}	0.01 ^{ns}	-0.11 ^{ns}	-0.28 ^{ns}	-	-
LE (W m ⁻²)	BRW	Open	-0.11	-0.13	0.00	0.17	0.00	0.05	0.01	0.05	0.05	0.00	-	-
	UAF	Open	0.58	0.73	0.42	0.16	-0.01	-	0.00	0.34	0.49	0.04	-	-
	TSE	Open	0.54	0.37	0.45	-0.54	-0.02	0.05	0.04	0.43	0.61	-0.14	-	-
		Closed	0.27	0.22	0.33	-0.29	0.02	-0.04	0.01	0.35	0.40	-0.48	-	1.87
	TMK	Open	0.10	0.09	0.01	0.86	-0.05	0.09	0.11	0.29	0.29	-0.18	-	-
		Closed	0.05	0.08	0.03	0.24	0.03	-0.02	0.01	0.34	0.19	0.40	-	2.54
	FHK	Open	0.35	0.35	0.17	0.37	-0.02	0.06	0.07	0.72	1.25	-0.04	-	-
		Closed	-0.43	0.51	0.55	1.30	0.02	0.06	0.02	0.86	1.23	0.64	-	2.39
	MSE	Open	0.30	0.06	0.36	0.89	-0.03	0.01	0.01	0.07	0.05	-0.57	-	-
		Closed	-1.56	-1.23	-0.39	0.94	0.01	-0.01	-0.01	0.19	-0.07	0.93	-	7.62
	PDF	Open	1.53	1.50	1.29	1.93	0.04	-	0.03	1.79	2.99	0.25	-	-
	Average ^a	Open	0.47 ^{ns}	0.42 ^{ns}	0.39 ^{ns}	0.55 ^{ns}	-0.02 ^{ns}	0.05*	0.04**	0.53 ^{ns}	0.82 ^{ns}	-0.09 ^{ns}	-	-
		Closed	-0.42 ^{ns}	-0.11 ^{ns}	-0.13 ^{ns}	0.55 ^{ns}	0.02*	0.00 ^{ns}	0.01 ^{ns}	0.43**	0.44 ^{ns}	0.37 ^{ns}	-	3.61**
		Both	0.15 ^{ns}	0.23 ^{ns}	0.29 ^{ns}	0.55 ^{ns}	0.00 ^{ns}	0.03 ^{ns}	0.03 ^{ns}	0.49 ^{ns}	0.68 ^{ns}	0.08 ^{ns}	-	3.61**
Fc (μmol m ⁻² s ⁻¹)	BRW	Open	0.00	0.00	-0.02	-0.06	0.02	0.10	0.00	-0.02	-0.02	0.00	0.05	-
	UAF	Open	-0.05	-0.16	-0.04	-0.12	0.07	-	0.01	-0.04	-0.06	-0.07	0.79	-
	TSE	Open	0.03	0.02	0.04	0.02	0.07	0.06	0.02	-0.02	-0.03	-0.12	0.36	-
		Closed	0.03	0.04	0.00	-0.19	-0.04	-0.05	-0.03	-0.05	-0.05	-0.27	-	-0.04
	TMK	Open	0.05	0.05	0.00	0.02	0.07	0.27	0.04	-0.04	-0.03	-0.03	0.46	-
		Closed	0.01	0.02	0.00	0.06	0.00	-0.01	0.04	0.00	0.00	-0.20	-	0.00
	FHK	Open	0.05	-0.02	-0.03	0.01	0.04	0.20	0.01	-0.08	-0.11	-0.01	0.33	-
		Closed	0.19	-0.01	-0.02	0.04	0.00	0.00	0.01	-0.04	-0.03	-0.10	-	0.25
	MSE	Open	-0.10	-0.05	0.02	-0.02	0.21	0.06	0.00	-0.01	-0.01	-0.07	0.56	-
		Closed	-0.14	-0.06	0.00	0.03	0.00	0.00	0.01	0.02	0.01	-0.19	-	-0.05
	PDF	Open	-0.16	-0.04	-0.01	0.11	0.28	-	0.02	0.05	0.10	0.11	0.09	-
	Average ^a	Open	-0.03 ^{ns}	-0.03 ^{ns}	-0.01 ^{ns}	0.00 ^{ns}	0.11**	0.14*	0.01**	-0.02 ^{ns}	-0.02 ^{ns}	-0.03 ^{ns}	0.38*	-
		Closed	-0.02 ^{ns}	-0.01 ^{ns}	0.00 ^{ns}	-0.02 ^{ns}	-0.01 ^{ns}	-0.02 ^{ns}	0.01 ^{ns}	-0.02 ^{ns}	-0.02 ^{ns}	-0.19*	-	0.04 ^{ns}
		Both	-0.01 ^{ns}	-0.02 ^{ns}	-0.01 ^{ns}	-0.01 ^{ns}	0.07 ^{ns}	0.07 ^{ns}	0.01 ^{ns}	-0.02 ^{ns}	-0.02 ^{ns}	-0.09 ^{ns}	0.38*	0.04 ^{ns}

^aSuperscripts of “ns”, “*”, and “**” represent that averaged intercept was statistically no significant from 0.0 ($p > 0.10$), significant ($p < 0.05$), and significant ($0.05 < p < 0.10$), respectively.

Table 6. Slope, intercept and R^2 values of linear regression between fluxes by open- and closed-path systems at the control experiment

Site	LE control (W m^{-2})			LE Mammarella (W m^{-2})			Fc control ($\mu\text{mol m}^{-2} \text{s}^{-1}$)		
	Slope	Intercept	R^2	Slope	Intercept	R^2	Slope	Intercept	R^2
FHK	1.05	3.33	0.93	1.01	4.13	0.9501	1.05	1.31	0.94
MSE	1.01	-19.51	0.95	0.91	-10.76	0.93	1.01	0.78	0.99
TMK	0.99	-4.51	0.92	1.12	3.44	0.93	1.02	0.84	0.96
TSE	0.93	-4.68	0.95	0.92	-2.14	0.96	0.94	1.01	0.97
Average	0.99	-6.34	0.94	0.99	-1.33	0.94	1.00	0.98	0.97
Interval	0.06	11.22	0.02	0.11	8.10	0.02	0.06	0.28	0.02

$30 \text{ g C m}^{-2} \text{ yr}^{-1}$ for NEE produced by the closed-path systems (PFR and DRext in Fig. 6; Table 7). By applying the TR, the systematic bias and random error in the half-hourly data were propagated to the annual fluxes (TR in Fig. 6 and Table 7); consequently, the application of TR induced large uncertainties in the annual fluxes. The TR significantly biased the annual NEE measured at sites in tall canopy (TMK, FHK and PDF; $132 \text{ g C m}^{-2} \text{ yr}^{-1}$, $p < 0.05$), even though the bias was insignificant at sites in small canopy (BRW, UAF, TSE and MSE).

Because the half-hourly H was strongly affected by corrections for crosswind (NoCW in Fig. 4) and water vapor (NoWV in Fig. 4), these corrections induced systematic biases in the annual H of $+2.4 \text{ W m}^{-2}$ (no water vapor correction; $p = 0.06$) and $+3.5 \text{ W m}^{-2}$ (no-crosswind correction; insignificant). The systematic bias of those corrections were propagated to the annual NEE through the WPL correction in the open-path systems (up to $+60 \text{ g C m}^{-2} \text{ yr}^{-1}$; $p < 0.09$). In contrast, the systematic bias of the no water vapor correction did not show the statistical significant bias in the annual NEE, probably because other errors, such as gap-filling and difference in survived data, were larger than the systematic bias of the no water vapor correction.

Despiking did not strongly influence the annual fluxes, except for NEE at PDF (NoDespike in Fig. 6 and Table 7); the annual uncertainties at other fluxes were less than few percentiles with no significant biases. The despiking increased the net annual sink at PDF by approximately $+206 \text{ g C m}^{-2} \text{ yr}^{-1}$ compared to that of the control calculation because a moderate relative reduction of RE (8%) substantially influenced absolute of RE ($271 \text{ g C m}^{-2} \text{ yr}^{-1}$) and GPP was less influenced by despiking (Fig. 6 and Table 7).

All the annual fluxes tended to decrease by no high-frequency loss correction (NoHL in Fig. 6). The biases in the closed-path systems were larger than those in the open-path systems (Table 7), indicating this correction is most sensitive and important in the closed-path systems.

Except for the PDF site, storage correction did not significantly induce systematic biases to NEE, GPP and RE

(Storage in Fig. 6). The storage correction had a substantial influence (more than 20%) in GPP and RE at PDF, probably because the tropical rainforest had large CO_2 storage within the tall canopy (26 m). Excluding PDF, the annual uncertainties from storage correction were $86 \text{ g C m}^{-2} \text{ yr}^{-1}$ for NEE, 8% for GPP and 17% for RE. The range of the annual uncertainties tended to be smaller than other correction options.

The relative humidity correction (the Mammarella correction) tended to increase ET by the closed-path systems on average of $+11\%$ (Fig. 7). Evapotranspiration by the closed-path systems without the Mammarella correction underestimated ET by the open-path systems for 6% at FHK, 27% at MSE, 26% at TMK and 30% at TSE. Those with the Mammarella correction still underestimate ET by the open-path systems for 6% at FHK, 27% at MSE, 8% at TMK and 15% at TSE.

The self-heating correction significantly biased the annual carbon balance ($+143 \text{ g C m}^{-2} \text{ yr}^{-1}$; $p < 0.05$) (Fig. 8 and Table 7). The influence in the annual carbon balance was greatest among all the corrections for the open-path systems. The effect was most substantial at the calm site UAF, where the self-heating correction decreased the annual carbon sink by $306 \text{ g C m}^{-2} \text{ yr}^{-1}$. To examine the self-heating correction at UAF further, we recalculated the correction term by replacing each of the meteorological data (solar radiation, outgoing longwave radiation, air temperature and wind speed) observed at UAF with those observed at TMK and found that the large influence of the self-heating correction at UAF was caused by air temperature. The lowest air temperature at the continental winter climate increased magnitude of the correction up to about $118 \text{ g C m}^{-2} \text{ yr}^{-1}$. Excluding the UAF sites, the systematic biases by this correction was $+116 \text{ g C m}^{-2} \text{ yr}^{-1}$ for NEE ($p < 0.05$).

The intrasite differences (\pm their 90% confidence intervals) between the open- and closed-path systems based on the average of four sites were $-413 \pm 189 \text{ g C m}^{-2} \text{ yr}^{-1}$ for NEE, $32 \pm 163 \text{ g C m}^{-2} \text{ yr}^{-1}$ ($2 \pm 10\%$) for GPP and $-381 \pm 158 \text{ g C m}^{-2} \text{ yr}^{-1}$ ($-33 \pm 14\%$) for RE; percentiles were calculated as the ratio of the difference

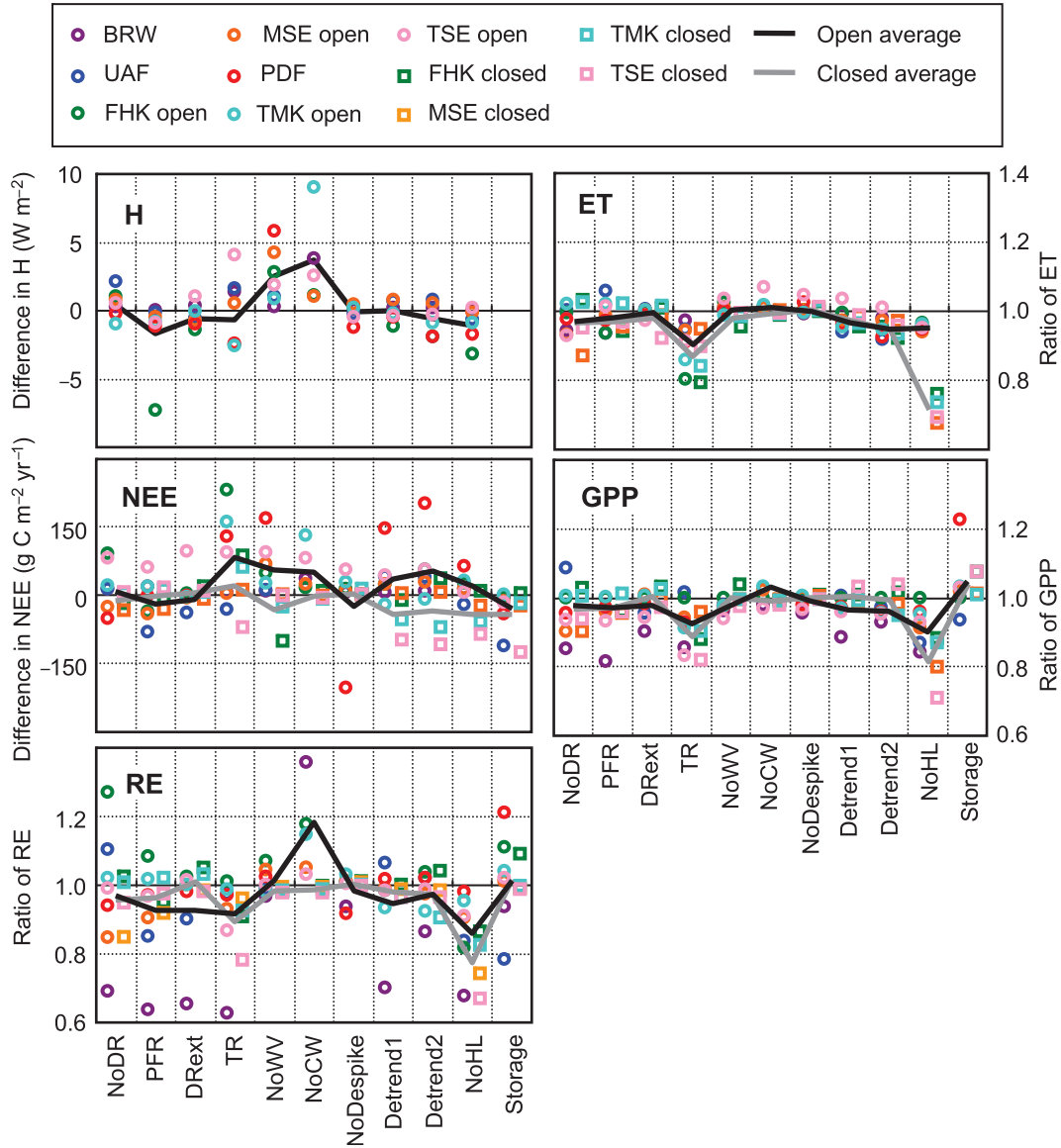


Fig. 6. Differences between the control and comparative calculations of the annual value of the sensible heat flux (H) and NEE as well as the ratios of the comparative to control calculations for the annual values of evapotranspiration (ET), gross primary productivity (GPP) and ecosystem respiration (RE). The positive bias in NEE means decrease in the sink or increase in the source.

compared to fluxes measured by the open-path systems. The difference was larger for NEE and RE compared with GPP. After the self-heating correction, the difference in NEE decreased, but the open-path systems still showed $280 \pm 166 \text{ g C m}^{-2} \text{ yr}^{-1}$ larger net carbon sink than the closed-path systems. The seasonal variations of NEE for the open- and closed-path systems are shown in Fig. 9. The self-heating correction decreased downward fluxes or increased upward fluxes throughout the season, but the following differences were found between the fluxes obtained via the open-path systems with the self-heating correction and the fluxes obtained by the closed-path

systems: (1) negative winter fluxes obtained using the open-path system were not fully corrected, and the open-path fluxes with the self-heating correction were still negative at TMK in March and at FHK from December to April; and (2) even after the correction, the negative fluxes in the growing season were larger in the open-path systems than those in the closed-path systems, except for MSE.

Finally, the annual uncertainties associated with various calculation options were taken as 90% confidence interval of each comparative annual flux for each site (excluding newly proposed corrections of the self-heating and the

Table 7. Differences between the control and comparative calculations of the annual value of the sensible heat flux (H) and NEE as well as the ratios of the comparative to control calculations for the annual values of evapotranspiration (ET), gross primary productivity (GPP) and ecosystem respiration (RE). The positive bias in NEE means decrease in the sink or increase in the source

Flux	Site	System	NoDR	PFR	DRext	TR	NoWV	NoCW	NoDespike	Detrend1	Detrend2	NoHL	Mammarella	Storage	SelfHeat
H (W m ⁻²)	BRW		0.3	0.0	0.4	1.4	0.3	3.8	0.0	0.2	0.2	-0.1	-	-	-
	UAF		2.1	-0.2	-0.6	1.6	1.0	-	-0.2	0.7	0.8	-0.6	-	-	-
	TSE		0.5	-0.9	1.0	4.0	1.8	2.5	-0.5	-0.4	-0.3	0.2	-	-	-
	TMK		-1.0	-0.9	-0.1	-2.6	0.9	9.0	0.2	-0.3	-1.0	-1.0	-	-	-
	FHK		1.0	-7.3	-1.4	-2.5	2.8	1.1	0.2	-1.1	-1.9	-3.2	-	-	-
	MSE		0.8	-0.5	-0.8	0.5	4.2	1.0	0.4	0.8	0.5	-0.2	-	-	-
	PDF		-0.3	-1.2	-1.0	-2.4	5.8	-	-1.2	-0.5	-1.9	-1.8	-	-	-
	Average ^a		0.5 ^{ns}	-1.6 ^{ns}	-0.4 ^{ns}	0.0 ^{ns}	2.4**	3.5 ^{ns}	-0.2 ^{ns}	-0.1 ^{ns}	-0.5 ^{ns}	-0.9 ^{ns}	-	-	-
	Interval ^b		1.9	5.0	1.7	5.0	3.9	7.0	1.1	1.3	2.1	2.3	-	-	-
ET (%)	BRW	Open	-5.8	-6.6	-0.2	-3.0	0.0	1.1	-1.1	-1.3	-2.2	-4.9	-	-	-
	UAF	Open	0.0	5.4	0.4	-5.5	0.7	-	-0.2	-6.4	-8.7	-4.9	-	-	-
	TSE	Open	-7.6	1.1	-3.0	-8.9	3.5	6.8	4.4	3.4	0.9	-5.2	-	-	-
		Closed	-5.2	-3.5	-8.2	-10.5	-0.8	-0.6	1.1	-1.5	-4.2	-30.9	21.9	-	-
	TMK	Open	1.8	1.8	0.0	-14.4	-1.6	1.6	-0.8	-4.6	-5.5	-4.0	-	-	-
		Closed	2.2	2.1	1.3	-16.0	-1.7	-0.9	0.0	-3.7	-6.6	-26.5	23.6	-	-
	FHK	Open	-0.6	-6.8	-0.2	-20.1	2.1	1.2	0.1	-0.7	-4.7	-3.5	-	-	-
		Closed	2.9	-6.1	0.6	-20.9	-4.5	-1.2	-0.3	-4.6	-8.0	-24.1	-0.2	-	-
	MSE	Open	-7.2	-1.6	-0.1	-5.8	0.8	0.8	0.1	-3.0	-2.9	-6.2	-	-	-
		Closed	-13.1	-4.7	-1.5	-5.4	-0.6	0.1	0.7	-1.6	-2.9	-32.5	-1.0	-	-
	PDF	Open	-2.7	-3.1	-1.6	-9.2	-0.1	-	2.2	-4.2	-7.7	-5.6	-	-	-
	Average ^a	Open	-3.1 ^{ns}	-1.4 ^{ns}	-0.7 ^{ns}	-9.5*	0.8 ^{ns}	2.3 ^{ns}	0.7 ^{ns}	-2.4 ^{ns}	-4.4*	-4.9*	-	-	-
		Closed	-3.3 ^{ns}	-3.0 ^{ns}	-1.9 ^{ns}	-13.2*	-1.9 ^{ns}	-0.6 ^{ns}	0.4 ^{ns}	-2.8*	-5.4*	-28.5*	11.1 ^{ns}	-	-
		Both	-3.2 ^{ns}	-2.0 ^{ns}	-1.2 ^{ns}	-10.9*	-0.2 ^{ns}	1.0 ^{ns}	0.6 ^{ns}	-2.6**	-4.8*	-13.5**	11.1 ^{ns}	-	-
	Interval ^b	Open	7.3	8.8	2.3	11.5	3.2	5.4	3.8	6.3	6.4	1.8	-	-	-
		Closed	17.6	8.5	10.1	15.7	4.3	1.3	1.5	3.6	5.5	9.1	31.8	-	-
		Both	9.1	7.4	4.7	11.1	3.8	4.4	2.8	4.8	5.3	22.0	31.8	-	-
NEE (g C m ⁻² yr ⁻¹)	BRW	Open	11.7	16.8	-3.8	5.4	6.8	35.4	5.7	4.5	7.1	13.2	-	-5.8	20.6
	UAF	Open	12.8	-82.0	-39.8	-31.8	10.6	-	7.9	41.1	37.2	-23.7	-	-112.4	305.9
	TSE	Open	80.5	59.3	96.0	93.3	91.6	80.8	54.0	41.7	54.5	4.9	-	-16.7	146.5
		Closed	6.7	17.1	7.7	-71.4	-0.4	-5.6	1.5	-98.9	-109.2	-87.1	-	-125.2	-
	TMK	Open	19.5	17.2	-5.5	161.1	24.1	129.9	26.3	-22.4	-9.5	30.9	-	1.0	161.3
		Closed	3.5	10.5	5.8	61.4	-25.7	-9.6	14.1	-53.0	-71.3	-59.4	-	-19.6	-
	FHK	Open	86.1	-41.2	2.5	224.8	47.7	11.2	13.7	18.4	51.6	25.4	-	-8.1	134.6
		Closed	-19.0	-6.9	19.8	87.1	-102.0	9.0	1.7	-12.2	36.2	7.9	-	4.1	-
	MSE	Open	-27.1	-42.8	-7.7	2.3	67.9	22.5	7.1	23.4	26.4	13.0	-	-14.5	180.1
		Closed	-34.1	-30.8	-9.0	10.7	2.0	-2.0	0.4	4.6	5.8	-23.6	-	-23.1	-

Table 7 (Continued)

Flux	Site	System	NoDR	PFR	DRext	TR	NoWV	NoCW	NoDespike	Detrend1	Detrend2	NoHL	Mammarella	Storage	SelfHeat
GPP (%)	PDF	Open	-52.7	-3.2	-3.0	126.3	168.0	-	-206.0	145.7	200.1	62.4	-	-41.3	51.9
	Average ^a	Open	18.7 ^{ns}	-10.8 ^{ns}	5.5 ^{ns}	83.1 ^{ns}	59.5**	55.9**	-13.1 ^{ns}	36.1 ^{ns}	52.5 ^{ns}	18.0 ^{ns}	-	-28.2 ^{ns}	143.0*
		Closed	-10.8 ^{ns}	-2.5 ^{ns}	6.1 ^{ns}	21.9 ^{ns}	-31.5 ^{ns}	-2.0 ^{ns}	4.4 ^{ns}	-39.9 ^{ns}	-34.6 ^{ns}	-40.5 ^{ns}	-	-40.9 ^{ns}	-
		Both	8.0 ^{ns}	-7.8 ^{ns}	5.7 ^{ns}	60.8 ^{ns}	24.6 ^{ns}	30.2 ^{ns}	-6.7 ^{ns}	8.5 ^{ns}	20.8 ^{ns}	-3.3 ^{ns}	-	-32.9 ^{ns}	143.0*
	Interval ^b	Open	99.2	92.3	82.1	184.2	110.6	104.6	168.6	103.3	134.2	51.1	-	76.6	180.2
		Closed	45.5	50.4	27.8	164.4	114.4	18.8	15.2	108.7	158.2	97.6	-	135.3	-
		Both	78.9	70.4	60.5	160.1	125.1	86.4	123.0	111.8	142.1	77.0	-	80.4	180.2
	BRW	Open	-14.8	-18.6	-9.8	-14.4	-3.8	-2.3	-4.4	-11.6	-7.3	-15.9	-	0.3	-10.6
	UAF	Open	8.7	-3.6	-4.4	1.7	-2.3	-	-0.4	0.5	-3.0	-13.3	-	-6.4	5.7
	TSE	Open	-6.4	-6.8	-5.7	-16.9	-6.4	-3.2	-3.5	-4.2	-4.8	-7.3	-	2.7	-10.7
		Closed	-6.2	-4.2	-2.9	-18.2	-2.6	-2.2	-0.5	3.2	3.7	-29.2	-	7.3	-
	TMK	Open	0.4	0.3	0.3	-9.0	-2.6	3.3	0.6	-3.3	-4.7	-4.8	-	3.1	-3.1
		Closed	0.4	1.0	2.4	-9.9	-0.5	-0.9	-0.7	-1.0	-5.4	-13.2	-	0.6	-
	FHK	Open	11.5	6.7	1.2	-10.1	1.8	9.6	0.0	-1.8	-0.2	-11.7	-	6.7	-4.8
		Closed	2.8	-3.9	2.9	-12.5	3.7	-0.8	0.7	0.6	1.3	-12.1	-	7.2	-
	MSE	Open	-9.9	-4.0	0.8	-5.7	-2.3	2.1	0.2	-2.8	-4.4	-8.7	-	2.0	-2.6
		Closed	-10.1	-4.6	-0.7	-4.5	-0.8	-0.6	0.3	-1.6	-2.2	-20.2	-	1.1	-
	PDF	Open	-4.6	-2.9	-2.0	-7.2	-2.9	-	-2.1	-3.0	-4.1	-4.1	-	22.7	2.4
	Average ^a	Open	-2.2 ^{ns}	-4.1 ^{ns}	-2.8 ^{ns}	-8.8*	-2.7*	1.9 ^{ns}	-1.4 ^{ns}	-3.7*	-4.1*	-9.4*	-	4.4 ^{ns}	-3.4 ^{ns}
		Closed	-3.3 ^{ns}	-2.9 ^{ns}	0.4 ^{ns}	-11.3*	-0.1 ^{ns}	-1.1*	-0.1 ^{ns}	0.3 ^{ns}	-0.6 ^{ns}	-18.7*	-	4.1 ^{ns}	-
		Both	-2.6 ^{ns}	-3.7 ^{ns}	-1.6 ^{ns}	-9.7*	-1.7 ^{ns}	0.5 ^{ns}	-0.9 ^{ns}	-2.3 ^{ns}	-2.8 ^{ns}	-12.8*	-	4.3 ^{ns}	-3.4 ^{ns}
	Interval ^b	Open	18.6	14.9	7.9	11.8	4.7	10.9	3.9	7.4	4.1	8.6	-	17.5	11.8
		Closed	14.0	6.2	6.3	13.4	6.3	1.7	1.6	5.0	9.3	18.6	-	8.7	-
		Both	14.7	11.2	7.0	10.5	4.9	7.4	3.1	6.8	5.9	13.1	-	13.2	11.8
RE (%)	BRW	Open	-30.9	-36.2	-34.5	-37.4	-3.3	35.6	-6.5	-30.0	-13.6	-32.4	-	-6.2	-7.3
	UAF	Open	10.4	-14.9	-9.9	-2.7	-0.9	-	0.7	6.2	2.1	-16.5	-	-21.8	47.7
	TSE	Open	-1.0	-3.5	1.2	-13.4	0.0	3.1	0.3	-1.7	-1.3	-9.1	-	2.0	-0.5
		Closed	-5.4	-2.8	-2.2	-22.0	-2.5	-2.5	-0.4	-3.7	-3.9	-33.4	-	-1.5	-
	TMK	Open	2.1	1.7	0.1	-1.3	-2.1	14.6	2.9	-6.7	-7.7	-4.8	-	3.9	7.5
		Closed	0.6	1.7	2.9	-7.7	-2.0	-1.5	0.0	-3.9	-9.7	-17.8	-	-0.3	-
	FHK	Open	27.0	8.2	2.3	1.0	7.0	17.5	1.2	-1.5	3.8	-18.2	-	11.0	2.8
		Closed	2.2	-5.1	4.7	-9.4	-2.1	-0.4	1.0	-0.1	3.9	-13.9	-	8.8	-
	MSE	Open	-15.4	-9.7	0.2	-7.0	4.4	5.0	1.1	-1.0	-2.8	-9.6	-	0.9	16.2
		Closed	-15.4	-8.6	-1.8	-4.1	-0.7	-1.0	0.3	-1.4	-1.9	-26.2	-	-1.1	-
	PDF	Open	-6.1	-2.9	-2.1	-3.2	2.3	-	-8.4	1.5	2.1	-2.1	-	21.1	4.0
	Average ^a	Open	-2.0 ^{ns}	-8.2 ^{ns}	-6.1 ^{ns}	-9.1 ^{ns}	1.1 ^{ns}	15.2*	-1.2 ^{ns}	-4.7 ^{ns}	-2.5 ^{ns}	-13.2*	-	1.5 ^{ns}	10.0 ^{ns}
		Closed	-4.5 ^{ns}	-3.7 ^{ns}	0.9 ^{ns}	-10.8*	-1.8*	-1.3*	0.2 ^{ns}	-2.3*	-2.9 ^{ns}	-22.8*	-	1.5 ^{ns}	-
		Both	-2.9 ^{ns}	-6.6 ^{ns}	-3.6 ^{ns}	-9.7 ^{ns}	0.0 ^{ns}	7.8 ^{ns}	-0.7 ^{ns}	-3.8 ^{ns}	-2.6 ^{ns}	-16.7*	-	1.5 ^{ns}	10.0 ^{ns}

Table 7 (Continued)

Flux	Site	System	NoDR	PFR	DRExt	TR	NoWV	NoCW	NoDespike	Detrend1	Detrend2	NoHL	Mammarella	Storage	SelfHeat
	Interval ^b	Open	35.8	28.0	25.6	25.8	7.2	27.6	8.4	22.9	12.1	19.9	–	26.1	35.2
		Closed	18.8	10.1	8.0	18.3	1.9	2.1	1.4	4.3	13.2	20.5	–	11.6	–
		Both	27.2	21.1	19.9	20.3	5.9	23.5	6.3	16.8	10.4	18.9	–	19.5	35.2

^aSuperscripts of “ns”, “*”, and “***” represent that averaged value was statistically no significant from the value by the control experiment ($p > 0.10$), significant ($p < 0.05$), and significant ($0.05 < p < 0.10$), respectively.

^bInterval represent 90% confidence interval (t -distribution) of change in the annual flux associated with the each calculation option.

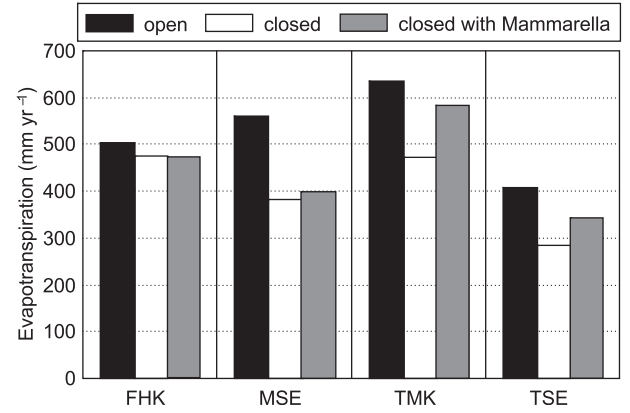


Fig. 7. Annual evapotranspiration (ET) by the open-path system, the closed-path system and the closed-path system correcting humidity effect on the high-frequency loss (Mammarella et al., 2009). Since the flux measurement by the closed-path system was only conducted between DOY105 and 294 at MSE, ET is only compared for that period.

Mammarella corrections) to account for the range of variations (dots in Fig. 10). The annual uncertainties were then averaged for all the sites (bar chart in Fig. 10). The annual uncertainties in the multisite data obtained associated with the flux calculation options were $3.4 \pm 1.5 \text{ W m}^{-2}$ for H, $95 \pm 61 \text{ g C m}^{-2} \text{ yr}^{-1}$ for NEE, $8 \pm 2\%$ of the annual total for ET, $10 \pm 3\%$ for GPP and $18 \pm 10\%$ for RE by the open-path systems, whereas those obtained by the closed-path systems were $65 \pm 34 \text{ g C m}^{-2} \text{ yr}^{-1}$ for NEE, $20 \pm 4\%$ of the annual total for ET, $12 \pm 5\%$ for GPP and $14 \pm 4\%$ for RE. Then, we quantified the uncertainties in preferred multisite data under current recommendation in the FLUXNET (Aubinet et al., 2000; AsiaFlux, 2007). Assuming that all the recommended processing were included, we standardized these flux calculation options by excluding detrending, TR, the self-heating correction and the Mammarella correction and by adopting despiking, corrections for crosswind, water vapor and high-frequency loss. The annual uncertainties in the standardized dataset for the open-path systems decreased to $2.6 \pm 2.7 \text{ W m}^{-2}$ for H, $65 \pm 39 \text{ g C m}^{-2} \text{ yr}^{-1}$ for NEE, $8 \pm 4\%$ of the annual total for ET, $13 \pm 8\%$ for GPP and $19 \pm 11\%$ for RE. Those in the closed-path systems also decreased to $85 \pm 55 \text{ g C m}^{-2} \text{ yr}^{-1}$ for NEE, $7 \pm 6\%$ of the annual total for ET, $10 \pm 6\%$ for GPP and $9 \pm 8\%$ for RE.

To clarify how errors in the half-hourly fluxes propagated to the annual fluxes through the gap-filling processes, we applied gap-filling of the carbon fluxes to all comparative dataset by using u^* -threshold values and parameters for the non-linear regression models that were determined in the control experiment. The obtained annual uncertainties in the standardized dataset were $57 \pm 25 \text{ g C m}^{-2} \text{ yr}^{-1}$ for NEE, $5 \pm 3\%$ for GPP and $3 \pm 2\%$ for RE for the

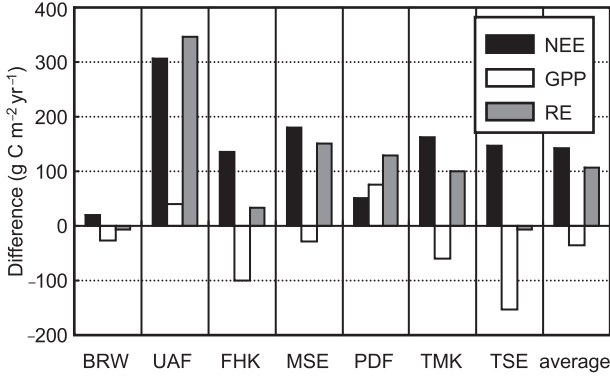


Fig. 8. Difference between annual fluxes with and without the self-heating correction by Amiro (2010). Positive values represent an increase of the fluxes (decreased CO₂ uptake) after the correction.

open-path systems and 93 ± 74 g C m⁻² yr⁻¹ for NEE, $11 \pm 4\%$ for GPP and $1 \pm 2\%$ for RE for the closed-path systems. The results indicated that part of the uncertainties in NEE (8 g C m⁻² yr⁻¹ by the open-path systems and 10 g C m⁻² yr⁻¹ by the closed-path systems) was amplified in the gap-filling processes, but the most of the annual uncertainties in NEE was directly from survived data rather than gap-filled data. The small influence by the gap-filling process was partly caused by fact that u^* -threshold was less sensitive to the flux correction option (the uncertainties were 0.03 ± 0.02 m s⁻¹; Fig. 10).

5. Discussion

In this study, we recalculated the fluxes at seven sites from 10-Hz raw data by applying various sets of flux calculation methods; this was done to evaluate the uncertainties in fluxes associated with these options that are present in the current FLUXNET database and other multisite databases. It should be noted that the uncertainties used in this study do not represent the uncertainties of individual eddy flux measurements but rather correspond to possible variabilities in the calculated fluxes originating from the flux calculation options. In our experimental design, u^* -threshold determination and quality control were conducted for each comparative dataset; thus, part of the annual uncertainties could have been propagated from differences in data surviving after the u^* -filtering and quality control procedures, in addition to the direct systematic effect of the flux calculation options.

Although the random sampling error must be small at annual timescale (less than 2%; Mano et al., 2007a), the annual uncertainties in the standardized fluxes showed a weak negative correlation with wind speed for the open-path systems ($R^2 = 0.56$ and $p = 0.06$). This weak dependence of NEE likely occurred due to increase in random error associated with low wind speed. This sensitivity to wind speed was probably caused by propagation of the random error because the random sampling errors were large under low-wind conditions (Richardson et al., 2006).

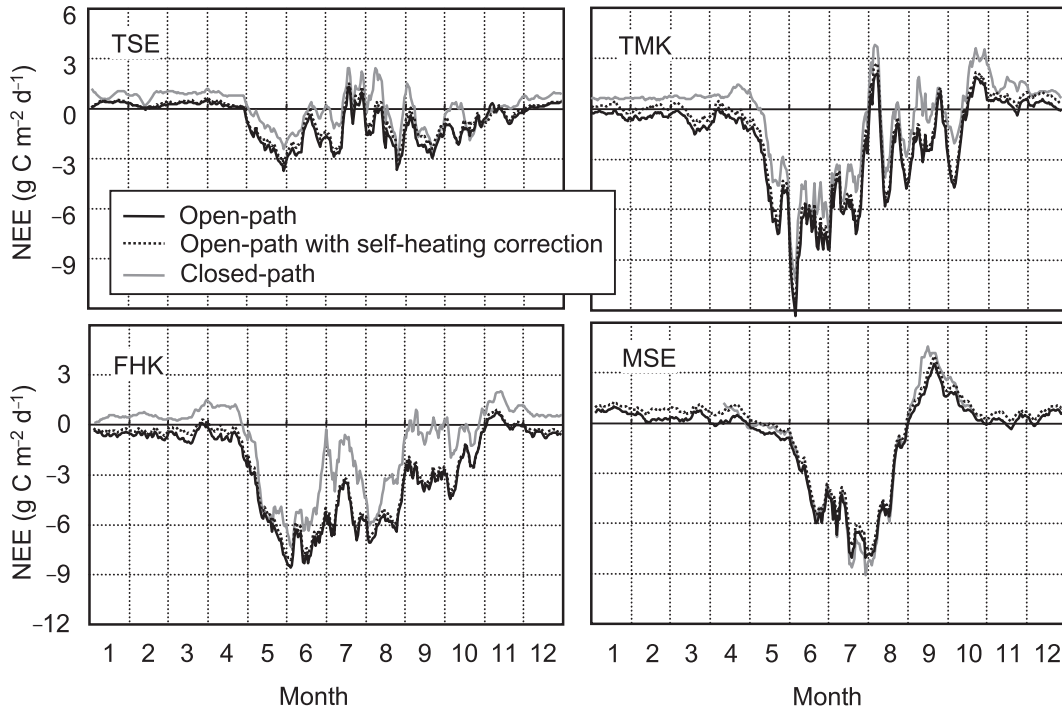


Fig. 9. Seasonal variations of NEE obtained by the open- and closed-path eddy covariance systems.

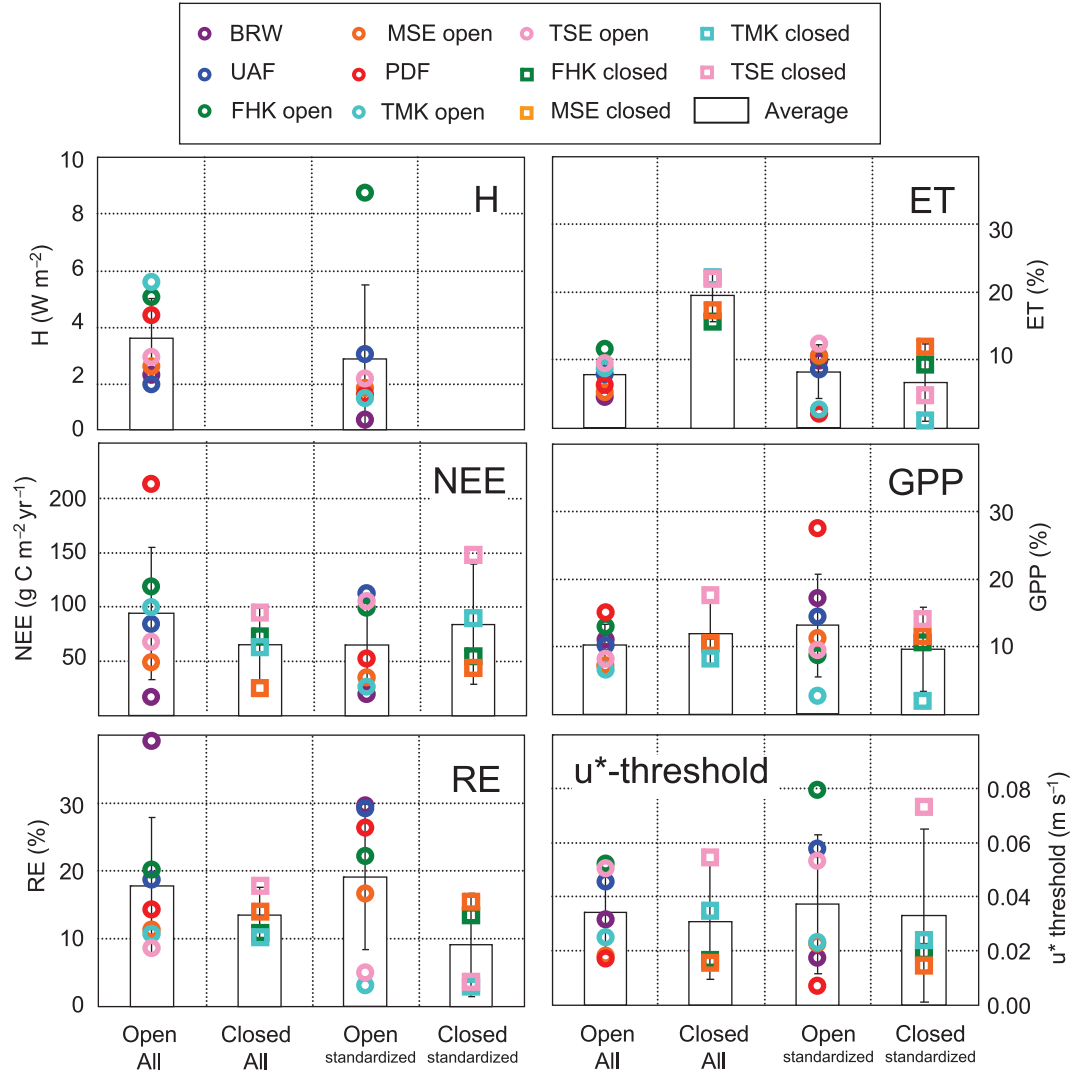


Fig. 10. Uncertainties of the annual fluxes and u^* -threshold caused by the flux calculation options. Points and bar charts represent the annual uncertainties for each site and mean, respectively, whereas vertical bars represent the 90% confidence interval. The uncertainties are categorized for the annual uncertainties associated with all of the corrections, except the self-heating and Mammarella corrections. The uncertainties from the standardized data are also shown in the figure, where the uncertainties at all recommended correction was applied (applying despiking, water vapor correction and crosswind correction, high-frequency loss and not applying detrending, TR, the self-heating correction and the Mammarella correction). Uncertainties for H, NEE and u^* -threshold are shown as differences, whereas those for ET, GPP and RE are shown as relative values.

This result indicates that calm sites tend to exhibit large uncertainties associated with flux calculation options due to the propagation of random errors.

The application of TR induced large random and systematic errors on a half-hourly basis and strongly biased annual fluxes at all of the sites, which was not observed for other rotation corrections. This effect was probably caused by large run-to-run variability in lateral stress measurements (Wilczak et al., 2001). Finnigan (2004) also noted that TR cannot be applied to real complex flows. Although this correction has rarely been applied in flux studies of

terrestrial ecosystems, we recommend that TR should not be applied except in case where this rotation is necessary for particular reasons; based on our analysis, flux data to which TR has been applied should be used with caution in multisite syntheses. Except for the TR correction, we found that the choice of rotation options mostly did not affect half-hourly and annual fluxes, indicating that there was no serious bias caused by the choice of coordinate rotation in the current multisite flux database. The topography was simple at all of our study sites. Because fluxes on complex topography might be influenced by rotation corrections,

further studies are required to understand the effect of rotation for flux sites with complex topographies.

Corrections for water vapor fluctuation and crosswind to virtual air temperature were highly influential with respect to the sensible heat fluxes obtained on both half-hourly and annual bases. The biased sensible heat flux systematically influenced the half-hourly and annual CO_2 fluxes through the WPL and frequency corrections. The water vapor correction had a greater effect at the humid sites MSE (rice paddy) and PDF (tropical swamp forest). For these humid sites, the half-hourly H was sometimes close to zero during the day; in such cases, small changes in H from positive to negative (or vice versa) associated with the corrections strongly influenced LE and F_c through the correction by the theoretical transfer function because it depends on atmospheric stability.

Detrending decreased half-hourly fluxes (Figs. 4 and 5). This decrease could be caused by an underestimation of low-frequency flux contributions associated with applying detrending procedure (Aubinet et al., 2003; Moncrieff et al., 2004). Although we corrected the low-frequency loss associated with linear detrending by applying a theoretical transfer function (Massman, 2000), the examined decrease in half-hourly fluxes may indicate that the correction was not sufficient. Despite this possible underestimation of the low-frequency flux contributions, a considerable number of studies based on long-term observations have applied the detrending procedure (e.g. Nakai et al., 2003; Kato and Tang, 2008). Thus, we should consider the resultant difference when we compare fluxes applied with detrending or with no detrending procedure because the option of detrending might cause a systematic bias.

The self-heating correction for the open-path sensor strongly influenced the annual carbon balance not only for cold sites but also for warm sites. The effect of the correction was substantially larger compared with the other calculation options and inevitably decreased carbon sinks or increased sources. After Burba et al. (2008) showed the necessity of the correction and proposed a set of equations for this self-heating correction, it was applied to several flux studies (e.g. Reverter et al., 2010), although it was not prudently applied to avoid a systematic bias at most sites (e.g. Bowling et al., 2010). Our results indicate that eddy flux datasets with and without this correction should be treated separately in current multisite synthesis. Amiro (2010) investigated the effect of this correction in three Canadian boreal forest sites and found that the effect was $210 \pm 20 \text{ g C m}^{-2} \text{ yr}^{-1}$. Reverter et al. (2011) reported that the effect ranged from 129 to $190 \text{ g C m}^{-2} \text{ yr}^{-1}$ among seven ecosystems in Spain. The effect of the correction reported in previous studies was similar to the effect estimated in the present study ($143 \pm 180 \text{ g C m}^{-2} \text{ yr}^{-1}$).

Although Reverter et al. (2011) demonstrated the possibility of predicting the effect from annual air temperature via a simple linear regression, we could not find a similar relationship, indicating that the influence of this correction on air temperature was different in each climate region. The effect estimated in our study represents the potential maximum of the correction because we assumed that the open-path sensor was installed with a vertical orientation. The actual effect of self-heating must be smaller because the open-path sensors were mounted at an angle from the vertical at most of our sites, except for FHK, as well as at the study sites of Amiro (2010). Unfortunately, the correction techniques for tilted open-path sensors are currently not available (Burba et al., 2008).

The differences between the open- and closed-path systems were large in the carbon fluxes and did not become negligible even when the self-heating correction was applied (Figs. 7 and 9; Table 3). Compared with the previous study ($25 \text{ g C m}^{-2} \text{ yr}^{-1}$ greater sink in the open-path system with the self-heating correction than in the closed-path system; Haslwanter et al., 2009), the values we determined for NEE (larger sink by the open-path systems for $413 \pm 189 \text{ g C m}^{-2} \text{ yr}^{-1}$ and $280 \pm 166 \text{ g C m}^{-2} \text{ yr}^{-1}$ without and with the self-heating correction, respectively) were considerably larger. The difference between the both systems was mostly caused by smaller estimates of RE (thus, nighttime F_c) in the open-path systems rather than larger estimates of GPP (Table 3), indicating the importance in accurate measurements in nighttime NEE. Our results indicate that the difference between the two systems varies greatly from site to site, and thus, careful consideration is necessary to synthesize the data from the two eddy covariance systems.

Without correcting the humidity effect in closed-path systems (Ibrom et al., 2007; Mammarella et al., 2009), the evaluated differences in annual ET between the open- and closed-path systems were similar to those observed in a previous study for a single site (Haslwanter et al., 2009); the ET value obtained via the closed-path system was 84 mm yr^{-1} less than that observed by the open-path system. After applying this correction, the underestimation decreased, but the ET by closed-path systems still underestimated the annual ET by the open-path systems. The effect of the correction on the annual fluxes also differed between the sites. After this correction, the underestimation was smaller in the forest sites (FHK and TMK) than in the low vegetation sites (MSE and TSE), which could indicate that the high-frequency attenuation depends on vegetation and/or measurement height. As shown in the NEE, the ET by the open- and closed-path systems must carefully be considered in synthesis using multisite data.

After standardising the recommended calculation options in the FLUXNET communities (Aubinet et al., 2000; AsiaFlux, 2007), the uncertainties associated with the flux

calculation options ($72 \pm 37 \text{ g C m}^{-2} \text{ yr}^{-1}$ for NEE) were comparable to other uncertainties associated with the accumulation of total random error (Richardson and Hollinger, 2005, $\pm 25 \text{ g C m}^{-2} \text{ yr}^{-1}$), the u^* -threshold method ($15\text{--}100 \text{ g C m}^{-2} \text{ yr}^{-1}$ for NEE, within 10% for GPP and RE, Papale et al., 2006; $77 \text{ g C m}^{-2} \text{ yr}^{-1}$ for NEE, Falge et al., 2001), flux-partitioning ($52 \text{ g C m}^{-2} \text{ yr}^{-1}$ for NEE, $52 \text{ g C m}^{-2} \text{ yr}^{-1}$ for GPP and $87 \text{ g C m}^{-2} \text{ yr}^{-1}$ for RE, Lasslop et al., 2010), gap-filling (within $200 \text{ g C m}^{-2} \text{ yr}^{-1}$ for NEE, Falge et al., 2001; and $25 \text{ g C m}^{-2} \text{ yr}^{-1}$ for NEE, Moffat et al., 2007) and different eddy flux software ($150 \text{ g C m}^{-2} \text{ yr}^{-1}$ for NEE, Takagi et al., 2008). Because recent studies have standardized the quality control of data (Vickers and Mahrt, 1997), gap-filling (Falge et al., 2001), u^* -threshold determination (Gu et al., 2005; Reichstein et al., 2005) and flux partitioning (Reichstein et al., 2005), the uncertainties associated with these methods could be reduced in network studies (Hirata et al., 2008; Grant et al., 2009).

The examined uncertainties associated with flux calculation options should be considered in current multisite syntheses (e.g. Baldocchi et al., 2001; Hirata et al., 2008) because the half-hourly data in the current FLUXNET database have been processed individually by site managers at each site (Lasslop et al., 2010). The uncertainties estimated in this study were still small compared to those arising from other methods, and thus the eddy covariance technique has an advantage with respect to elucidating biosphere–atmosphere interactions (Loescher et al., 2006; Baldocchi, 2008). Additional validation using independent measurements will help to reduce the uncertainties in the eddy covariance technique.

6. Conclusion

The influences of individual calculation options on half-hourly fluxes were mostly within 10% of each other, as previously reported based on a similar analysis (Mauder et al., 2007, 2008; Nemitz et al., 2009). Some of the biases in half-hourly fluxes were amplified in annual fluxes because of the accumulation of small systematic errors. The high-frequency attenuation correction for the closed-path systems was most influential in the half-hourly and annual ET. The self-heating correction for open-path systems was the most influential calculation option, and thus, datasets that apply these corrections should be addressed with caution in multisite syntheses. Differences between the open- and closed-path systems were evident even when the self-heating correction was applied, indicating that careful consideration is necessary in synthesising data from these two measurement systems. To accurately evaluate long-term terrestrial fluxes and their spatial patterns, the sensitivities of the fluxes to these influential calculation

options should be considered carefully, even though the effect of the calculation options was not substantial on a half-hourly time scale.

To further improve the processing methods associated with the eddy covariance technique, the establishment of a framework to calculate fluxes from raw data by using single eddy-flux software is required. An open-source framework is helpful to standardize data processing. The future improvement of uncertainty assessment in this manner will result in the eddy covariance technique becoming more rigorous and will improve our understanding of terrestrial biosphere–atmosphere interactions.

7. Acknowledgements

We thank all of the individuals who contributed to the field observations and the development of the flux software. We also thank Dr. H. Iwata at the International Arctic Research Center of the University of Alaska, Fairbanks, for checking our flux software. Dr. Georg Mag. Wohlfahrt at the University of Innsbruck and two anonymous reviewers provided constructive comments on an earlier version of the manuscript. This study was partly supported by KAKENHI (20880025) and the JSPS A3 Foresight Program (CarboEastAsia).

8. Appendix A

A.1. High frequency loss correction for closed-path systems

High frequency loss for closed-path systems are corrected with an empirical transfer function (TF_{HF}) proposed by Aubinet et al. (2000). Empirical transfer function is determined by using observed normalized cospectra for scalar (C_{WS}) and air temperature (C_{WT}):

$$TF_{\text{HF}}(f) = \frac{C_{\text{WS}}(f)}{C_{\text{WT}}(f)}, \quad (1)$$

where f is frequency. The empirical transfer function is determined as follows:

$$TF_{\text{HF}} = \exp \left\{ -0.347 \left(\frac{f}{f_{\text{co}}} \right)^2 \right\}, \quad (2)$$

where f_{co} is an empirical constant explaining the cutoff frequency. In this study, two different f_{co} were empirically determined for CO_2 and water vapor at each site. To exclude the low-frequency attenuation effects, the empirical transfer functions were determined for $f > 0.01 \text{ Hz}$. In order to account cospectral formulation associated with atmospheric stability, we used an empirical cospectral model proposed by Moore (1986).

The relative humidity effect to high-frequency loss (Ibrom et al., 2007) is corrected according to Mammarella et al. (2009). By using all the quality checked turbulent fluctuation data (1-year data), relationship between f_{co} for H_2O and relative humidity is examined for each site:

$$\tau_{H_2O} = a + b \left(\frac{RH}{100} \right)^c, \quad (3)$$

where, a , b and c are empirical constants that are derived from least square method, RH is relative humidity (in percent) and τ_{H_2O} is $1/f_{co}$ for H_2O . For all our closed-path systems, the equation well explained the relationship (R^2 values were greater than 0.98).

9. Appendix B

B.1. Quality control

We applied a quality test to remove half-hourly flux data that included noise caused by rain, snow or fog. Steady state (instationary) and integral turbulence tests (Foken and Wichura, 1996) were applied as routine treatments. The criteria for discarding flux data were set at 50% for the steady state test and at 500% for the integral turbulence test. According to the higher moment test (Vickers and Mahrt, 1997; Mano et al., 2007b), we screened out data when the absolute value of skewness was greater than 3.6 and when the value of kurtosis was greater than 14.4. After these routine treatments, we manually excluded the remaining outliers. These quality tests were applied independently to each of the datasets produced by the experiments shown in Table 2. For consistency among each processed dataset, the manually excluded data point in some processed dataset was excluded in every other processed dataset, even though the data point seems to be good quality in other processed dataset. The data coverage after the quality control to the total data point is shown in Table A1. On average, 55.9% for H, 43.6% for LE and 46.2% for CO_2 flux survived after the quality control.

10. Appendix C

C.1. u^* -filtering correction

Using a u^* -threshold criterion (Aubinet et al., 2000), nighttime data obtained under calm conditions were screened out in this analysis. According to the algorithm of Reichstein et al. (2005), the u^* -threshold was derived specifically for each site and each dataset using a 95% threshold criterion—*The threshold is defined as the u^* -class where the night-time flux reaches more than 95% of the average flux at the higher u^* -classes. The threshold is only accepted if for the temperature class, temperature and u^* are*

not or only weakly correlated ($|r| < 0.4$). The final threshold is defined as the median of the thresholds of the (up to) six temperature classes. This procedure is applied to the subsets of four 3-month periods to account for seasonal variation of vegetation structure. For each period, the u^ -threshold is reported, but the whole data set is filtered according to the highest threshold found (conservative approach).* We defined nighttime data as data observed when the photosynthetic photon flux density (PPFD) was less than $10 \mu\text{mol m}^{-2} \text{s}^{-1}$. Although Reichstein et al. (2005) set the minimum u^* -threshold to 0.1 m s^{-1} , we did not apply any minimum threshold. After this u^* -filtering, $67 \pm 10\%$ of the nighttime data were excluded from the analyses.

11. Appendix D

D.1. Flux partitioning and model parameterisations

To parameterise the daytime CO_2 flux (F_c), we determined parameters for an empirical model consisting of the non-rectangular hyperbola functions (Prioul and Chartier, 1977):

$$F_c = \frac{-\phi Q - P_{\max} + \sqrt{(\phi Q + P_{\max})^2 - 4\phi Q \theta P_{\max}}}{2\theta} + R_d \quad (4)$$

Here, Q , P_{\max} , ϕ , θ and R_d are the PPFD, the maximum photosynthetic rate, the initial slope for the non-rectangular hyperbola, the convexity of the light-response curve and dark respiration, respectively. θ was set to 0.9 (Hirata et al., 2008). The parameters P_{\max} , ϕ and R_d were determined for each day for a 15-d moving window by the least-squares method.

Using the nighttime CO_2 flux data, we parameterized a commonly used empirical model, the exponential Lloyd and Taylor model (e.g. Lloyd and Taylor, 1994; Reichstein et al., 2005). In this model, ecosystem respiration (R_E), RE , is a function of air temperature (T_a) as determined based on the following equation:

$$R_E = R_{\text{ref}} \times \exp \left[\frac{E_0}{R} \left(\frac{1}{T_k + T_{\text{ref}} - T_0} - \frac{1}{T_k + T_a - T_0} \right) \right] \quad (5)$$

In the model, R_{ref} is simply a scale parameter. In eq. (5), E_0 is the activation energy, and R is the ideal gas constant. T_k , T_0 and T_{ref} are 273.15 K, 227.13 K and 10°C , respectively (Hirata et al., 2008). Using nighttime data, the parameters R_{ref} and E_0 were determined for each day for a 29-d moving window by the least-squares method. Daytime RE was extrapolated from T_a using eq. (5). The GPP was determined as the difference between the observed F_c and calculated RE . At the site MSE, the windows for the

Table A1. Data coverage (%) after the quality control to the total number of data point

	Control	NoDR	PFR	DRExt	TR	NoWV	NoCW	NoDespike	Detrend1	Detrend2	NoHL	Average
<i>BRW</i>												
H	75.4	69.8	68.8	71.8	68.7	75.5	75.4	66.1	78.5	79.4	75.4	73.2
LE	54.5	51.1	50.8	52.7	48.7	54.6	55.3	42.8	60.2	62.2	54.5	53.4
Fc	54.7	51.3	50.9	52.8	49.1	54.7	55.5	45.2	62.3	60.3	54.7	53.8
<i>UAF</i>												
H	50.8	61.4	56.5	56.3	49.8	51.5	–	50.5	55.6	57.5	50.8	54.1
LE	32.5	36.0	32.7	34.7	30.3	32.7	–	31.1	41.5	38.6	32.5	34.3
Fc	33.0	36.5	33.2	35.1	30.9	33.1	–	31.7	41.6	38.9	33.0	34.7
<i>TSE open</i>												
H	36.6	35.0	40.8	39.5	45.3	47.7	47.0	47.6	50.8	51.4	36.6	43.5
LE	23.5	23.7	26.3	25.9	29.4	31.1	30.9	28.6	28.5	28.8	23.5	27.3
Fc	23.7	23.9	26.5	26.1	29.7	31.3	31.1	28.8	29.0	28.7	23.7	27.5
<i>TSE closed</i>												
H	43.5	47.8	47.9	39.5	45.3	47.7	47.0	47.6	50.8	51.4	43.5	46.5
LE	45.0	50.8	50.7	42.1	47.7	49.8	50.1	49.3	49.2	49.6	46.9	48.3
Fc	42.6	47.6	47.6	41.2	45.1	46.8	46.9	46.1	42.6	43.0	42.6	44.7
<i>TMK open</i>												
H	64.5	61.2	64.9	64.5	60.3	54.3	64.8	64.7	67.6	68.7	64.5	63.6
LE	46.6	44.5	46.6	46.2	41.2	40.8	46.6	43.3	47.1	47.9	46.6	45.2
Fc	48.9	46.6	48.9	48.6	44.9	42.7	48.8	45.3	49.7	50.2	48.9	47.6
<i>TMK closed</i>												
H	64.5	61.2	64.9	64.5	60.3	54.3	64.8	64.7	67.6	68.7	64.5	63.6
LE	60.3	56.6	60.6	37.4	52.7	48.7	60.9	60.6	58.2	58.8	68.3	56.7
Fc	66.7	62.4	66.5	66.4	59.9	55.3	66.9	65.8	56.5	56.8	66.7	62.7
<i>MSE open</i>												
H		56.6	58.6	62.0	57.9	60.2	60.1	60.1	64.2	65.5	60.1	60.5
LE	50.5	47.5	49.4	51.7	48.4	50.7	50.5	49.3	54.8	56.1	50.5	50.8
Fc	50.7	47.8	49.7	52.0	48.9	50.9	50.7	49.5	54.9	56.2	50.7	51.1
<i>MSE closed</i>												
H	60.1	56.6	58.6	62.0	57.9	60.2	60.1	60.1	64.2	65.5	60.1	60.5
LE	46.0	43.3	46.9	48.7	43.4	46.0	46.5	45.8	47.4	48.4	61.5	47.6
Fc	60.2	57.8	61.0	62.4	56.7	60.2	60.2	59.6	62.6	63.6	60.2	60.4
<i>FHK open</i>												
H	47.3	46.5	46.6	48.2	42.6	46.9	41.5	47.3	51.4	52.9	47.3	47.1
LE	30.9	30.4	30.9	31.6	26.0	30.9	27.2	30.4	33.4	34.9	30.9	30.7
Fc	34.0	33.5	33.8	34.8	30.4	34.0	29.8	33.6	35.6	36.7	34.0	33.6
<i>FHK closed</i>												
H	47.3	46.5	46.6	48.2	42.6	46.9	41.5	47.3	51.4	52.9	47.3	47.1
LE	43.6	41.7	41.9	43.8	37.7	43.7	37.6	43.6	44.7	45.9	47.4	42.9
Fc	45.9	44.2	45.5	46.2	40.1	46.0	39.7	45.7	44.5	45.9	45.9	44.5
<i>PDF</i>												
H	56.8	56.3	57.0	57.5	54.6	56.6	–	47.3	59.3	60.5	56.8	56.3
LE	46.4	46.2	46.9	47.2	44.0	46.5	–	38.2	50.5	52.0	46.4	46.4
Fc	48.0	47.8	48.4	48.7	46.1	48.0	–	39.5	51.4	52.6	48.0	47.8
<i>Average</i>												
H	55.2	54.4	55.6	55.8	53.2	54.7	55.8	54.8	60.1	61.3	55.2	56.0
LE	43.6	42.9	44.0	42.0	40.9	43.2	45.1	42.1	46.9	47.6	46.3	44.0
Fc	46.2	45.4	46.5	46.8	43.8	45.7	47.8	44.6	48.3	48.4	46.2	46.2

parameterisation of GPP and RE were separated by considering the field management applied, such as transplanting, harvesting and drainage, because these management practices cause discontinuities in GPP and RE.

12. Appendix E

E.1. Gap-filling

The gaps in the half-hourly flux data were filled using a standardized method (Falge et al., 2001; Reichstein et al., 2005) to calculate annual fluxes. First, linear interpolation was applied for small gaps, i.e. those shorter than 2.0 h. Second, the look-up-table (LUT) method was applied if meteorological data [PPFD, T_a and the vapor pressure deficit (VPD)] were available. An LUT was created each day for a 15-d moving window; PPFD, T_a and VPD were classified into 26 classes from 10 to 2400 $\mu\text{mol m}^{-2} \text{s}^{-1}$, from -25 to 35°C and from 0 to 12.5 kPa, respectively. If VPD was not applicable, an LUT was created from PPFD and T_a ; if neither VPD nor T_a were available, an LUT was created from the PPFD alone. Third, for the CO_2 flux data, if the LUT method was not applicable, a non-linear regression method based on eqs. (4) and (5) was applied. Finally, if none of the above methods was applicable, a mean diurnal variation method was applied: the diurnal pattern was determined for each day for a 15-d moving window. There were no long-term gaps greater than 10 d for any of the sites in the datasets that were used in this study, except for the CO_2 and water vapor fluxes in mid-winter at the BRW and UAF sites. Thus, most gaps of the data resulted from the QC criteria described in Appendix B, and these gaps were mostly filled by the LUT method.

References

- Acevedo, O. C., Moraes, O. L. L., Degrazia, G. A., Fitzjarrald, D. R., Manzi, A. O. and co-authors. 2009. Is friction velocity the most appropriate scale for correcting nocturnal carbon dioxide fluxes? *Agric. Forest Meteorol.* **149**, 1–10.
- Amiro, B. 2010. Estimating annual carbon dioxide eddy fluxes using open-path analyzers for cold forest sites. *Agric. Forest Meteorol.* **150**, 1366–1372.
- AsiaFlux Steering Committee (ed.). 2007. *Practice of Flux Observations in Terrestrial Ecosystems*. Sapporo, Japan: Hokkaido Research Center, Forestry and Forest Products Research Institute
- Aubinet, M., Clement, R. C., Elbers, J. A., Foken, T., Grelle, A. and co-authors. 2003. Methodology for data acquisition, storage, and treatment. In: *Fluxes of Carbon, Water and Energy of European Forests* (ed. R. Valentini), Springer-Verlag, Berlin, pp. 9–35.
- Aubinet, M., Grelle, A., Ibrom, A., Rannik, Ü., Moncrieff, J. and co-authors. 2000. Estimates of the annual net carbon and water vapor exchange of forests: the EUROFLUX methodology. *Adv. Ecol. Res.* **30**, 113–175.
- Baldocchi, D. D. 2003. Assessing the eddy covariance technique for evaluating carbon dioxide exchange rates of ecosystems: past, present and future. *Global Change Biol.* **9**, 479–492.
- Baldocchi, D. 2008. ‘Breathing’ of the terrestrial biosphere: lessons learned from a global network of carbon dioxide flux measurement system. *Aust. J. Bot.* **56**, 1–26.
- Baldocchi, D. D., Falge, E., Gu, L., Olson, R., Hollinger, D. and co-authors. 2001. FLUXNET: a new tool to study the temporal and spatial variability of ecosystem-scale carbon dioxide, water vapor, and energy flux densities. *Bull. Am. Meteorol. Soc.* **82**, 2415–2434.
- Beer, C., Reichstein, M., Tomelleri, E., Ciais, P., Jung, M. and co-authors. 2010. Terrestrial gross carbon dioxide uptake: global distribution and covariation with climate. *Science* **329**, 834–838.
- Bowling, D. R., Bethers-Marchetti, S., Lunch, C. K., Grote, E. E. and Belnap, J. 2010. Carbon, water, and energy fluxes in a semiarid cold desert grassland during and following multiyear drought. *J. Geophys. Res.* **115**. DOI: 10.1029/2010JG001322.
- Burba, G. D., McDermitt, K., Grelle, A., Anderson, D. J. and Xu, L. 2008. Addressing the influence of instrument surface heat exchange on the measurements of CO_2 flux from open-path gas analyzers. *Global Change Biol.* **14**, 1851–1876.
- Falge, E., Baldocchi, D., Olson, R., Anthoni, P., Aubinet, M. and co-authors. 2001. Gap filling strategies for defensible annual sums of net ecosystem exchange. *Agric. Forest Meteorol.* **107**, 43–69.
- Finnigan, J. J. 2004. A re-evaluation of long-term flux measurement techniques part II: coordinate systems. *Bound. Lay. Meteorol.* **113**, 1–41.
- Finnigan, J. J., Clement, R., Malhi, Y., Leuning, R. and Cleugh, H. A. 2003. A re-evaluation of long-term flux measurement techniques. Part I: averaging and coordinate rotation. *Bound. Lay. Meteorol.* **107**, 1–48.
- Foken, T. and Wichura, B. 1996. Tools for quality assessment of surface-based flux measurements. *Agric. Forest Meteorol.* **78**, 83–105.
- Goulden, M. L., Munger, J. W., Fan, S.-M., Daube, B. and Wofsy, S. C. 1996. Measurements of carbon sequestration by long-term eddy covariance: methods and a critical evaluation of accuracy. *Global Change Biol.* **2**, 169–182.
- Grant, R. F., Arain, A., Arora, V., Barr, A., Black, T. A. and co-authors. 2005. Intercomparison of techniques to model high temperature effects on CO_2 and energy exchange in temperate and boreal coniferous forests. *Ecol. Model.* **188**, 217–252.
- Grant, R. F., Barr, A. G., Black, T. A., Margolis, H. A., Dunn, A. L. and co-authors. 2009. Interannual variation in net ecosystem productivity of Canadian forests as affected by regional weather patterns – a Fluxnet-Canada synthesis. *Agric. Forest Meteorol.* **149**, 2022–2039.
- Gu, L., Falge, E., Boden, T., Baldocchi, D. D., Black, T. A. and co-authors. 2005. Objective threshold determination for nighttime eddy flux filtering. *Agric. Forest Meteorol.* **128**, 179–197.
- Harazono, Y., Mano, M., Miyata, A., Zulueta, R. and Oechel, W. C. 2003. Inter-annual carbon dioxide uptake of a wet sedge tundra ecosystem in the Arctic. *Tellus* **55B**, 215–231.

- Haslwanter, A., Hammerle, A. and Wohlfahrt, G. 2009. Open-path vs. closed-path eddy covariance measurements of the net ecosystem carbon dioxide and water vapour exchange: a long-term perspective. *Agric. Forest Meteorol.* **149**, 291–302.
- Hignett, P. 1992. Corrections to temperature measurements with a sonic anemometer. *Bound. Lay. Meteorol.* **61**, 175–187.
- Hirano, T., Hirata, R., Fujinuma, Y., Saigusa, N., Yamamoto, S. and co-authors. 2003. CO₂ and water vapor exchange of a larch forest in northern Japan. *Tellus* **55B**, 244–257.
- Hirano, T., Segah, H., Harada, T., Limin, S., June, T. and co-authors. 2007. Carbon dioxide balance of a tropical peat swamp forest in Kalimantan, Indonesia. *Global Change Biol.* **13**, 412–425.
- Hirata, R., Hirano, T., Mogami, J., Fujinuma, Y., Inukai, K. and co-authors. 2005. CO₂ flux measured by an open-path system over a larch forest during the snow-covered season. *Phyton Ann. Rei Bot. A* **45**, 347–351.
- Hirata, R., Hirano, T., Saigusa, N., Fujinuma, Y., Inukai, K. and co-authors. 2007. Seasonal and interannual variations in carbon dioxide exchange of a temperate larch forest. *Agric. Forest Meteorol.* **147**, 110–124.
- Hirata, R., Saigusa, N., Yamamoto, S., Ohtani, Y., Ide, R. and co-authors. 2008. Spatial distribution of carbon balance in forest ecosystems across East Asia. *Agric. Forest Meteorol.* **148**, 761–775.
- Ibrom, A., Dellwik, E., Flyvbjerg, H., Jensen, N. O. and Pilegaard, K. 2007. Strong low-pass filtering effects on water vapour flux measurements with closed-path eddy correlation systems. *Agric. Forest Meteorol.* **147**, 140–156.
- Ito, A. 2008. The regional carbon budget of East Asia simulated with a terrestrial ecosystem model and validated using AsiaFlux data. *Agric. Forest Meteorol.* **148**, 738–747.
- Kaimal, J. C. and Gaynor, J. E. 1991. Another look at sonic thermometry. *Bound. Lay. Meteorol.* **56**, 401–410.
- Kato, T. and Tang, Y. 2008. Spatial variability and major controlling factors of CO₂ sink strength in Asian terrestrial ecosystems: evidence from eddy covariance data. *Global Change Biol.* **14**, 2333–2348.
- Lasslop, G., Reichstein, M., Papale, D., Richardson, A. D., Arneeth, A. and co-authors. 2010. Separation of net ecosystem exchange into assimilation and respiration using a light response curve approach: critical issues and global evaluation. *Global Change Biol.* **16**, 187–208.
- Lloyd, J. and Taylor, J. A. 1994. On the temperature dependence of soil respiration. *Funct. Ecol.* **8**, 315–323.
- Loescher, H. W., Law, B. E., Mahrt, L., Hollinger, D. Y., Campbell, J. and co-authors. 2006. Uncertainties in, and interpretation of, carbon flux estimates using the eddy covariance technique. *J. Geophys. Res.* **111**, D21S90. DOI: 10.1029/2005JD006932.
- Luyssaert S., Inglisma, I., Jung, M., Richardson, A. D., Reichstein, M. and co-authors. 2007. The CO₂-balance of boreal, temperate and tropical forests derived from a global database. *Global Change Biol.* **13**, 2509–2537.
- Luyssaert, S., Schulze, E. D., Borner, A., Knohl, A., Hessenmoller, D. and co-authors. 2008. Old-growth forests as global carbon sinks. *Nature* **55**, 213–215.
- Mammarella, I., Launiainen, S., Gronholm, T., Keronen, P., Pumpanen, J. and co-authors. 2009. Relative humidity effect on the high-frequency attenuation of water vapor flux measured by a closed-path eddy covariance system. *J. Atmos. Oceanic Technol.* **26**, 1856–1866.
- Mano, M., Miyata, A., Nagai, H., Yamada, T., Ono, K. and co-authors. 2007a. Random sampling errors in CO₂ fluxes measured by the open-path eddy covariance method and their influence on estimating annual carbon budget. *J. Agric. Meteorol.* **63**, 67–69.
- Mano, M., Miyata, A., Yasuda, Y., Nagai, H., Yamada, T. and co-authors. 2007b. Quality control for the open-path eddy covariance data. *J. Agric. Meteorol.* **63**, 125–138.
- Massman, W. J. 2000. A simple method for estimating frequency response corrections for eddy covariance systems. *Agric. Forest Meteorol.* **104**, 185–198.
- Massman, W. J. 2001. Reply to comment by Rannik on “A simple method for estimating frequency response corrections for eddy covariance systems”. *Agric. Forest Meteorol.* **107**, 247–251.
- Mauder, M. and Foken, T. 2006. Impact of post-field data processing on eddy covariance flux estimates and energy balance closure. *Meteorol. Z.* **15**, 597–609.
- Mauder, M., Desjardins, R., Pattey, E. and Worth, D. 2010. An attempt to close the surface energy balance using spatially-averaged flux measurements. *Geophys. Res. Abst.* **12**, EGU2010-2866.
- Mauder, M., Foken, T., Clement, R., Elbers, J. A., Eugster, W. and co-authors. 2008. Quality control of CarboEurope flux data – part 2: inter-comparison of eddy-covariance software. *Biogeosciences* **5**, 451–462.
- Mauder, M., Oncley, S. P., Vogt, R., Weidinger, T., Ribeiro, L. and co-authors. 2007. The energy balance experiment EBEX-2000. Part II: intercomparison of eddy-covariance sensors and post-field data processing method. *Bound. Lay. Meteorol.* **123**, 29–54.
- McMillen, R. T. 1988. An eddy correlation technique with extended applicability to non-simple terrain. *Bound. Lay. Meteorol.* **43**, 231–245.
- Moffat, A., Papale, D., Reichstein, M., Hollinger, D. Y., Richardson, A. D. and co-authors. 2007. Comprehensive comparison of gap-filling techniques for eddy covariance net carbon fluxes. *Agric. Forest Meteorol.* **147**, 209–232.
- Moncrieff, J., Clement, R., Finnigan, J. and Meyers, T. 2004. Averaging, detrending, and filtering of eddy covariance time series. In: *Handbook of Micrometeorology: A Guide for Surface Flux Measurement and Analysis* (eds. X. Lee, W. Massman and B. Law), Kluwer Academic Publishers, Dordrecht, pp. 7–31.
- Moore, C. J. 1986. Frequency response corrections for eddy correlation systems. *Bound. Lay. Meteorol.* **37**, 17–35.
- Nakai, T., van der Molen, M. K., Gash, J. H. C. and Kodama, Y. 2006. Correction of sonic anemometer angle of attack errors. *Agric. Forest Meteorol.* **136**, 19–30.
- Nakai, Y., Kitamura, K., Suzuki, S. and Abe, S. 2003. Year-long carbon dioxide exchange above a broadleaf deciduous forest in Sapporo, Northern Japan. *Tellus* **55B**, 305–312.
- Nemitz, E., Hargreaves, K. J., Neftel, A., Loubet, B., Cellier, P. and co-authors. 2009. Intercomparison and assessment of

- turbulent and physiological exchange parameters of grassland. *Biogeosciences* **6**, 1445–1466.
- Owen, K. E., Tenhunen, J., Reichstein, M., Wang, Q., Falge, E. and co-authors. 2007. Linking flux network measurements to continental scale simulations: ecosystem CO₂ exchange capacity under non-water-stressed conditions. *Global Change Biol.* **13**, 734–760.
- Papale, D., Reichstein, M., Aubinet, M., Canfora, E., Bernhofer, C. and co-authors. 2006. Towards a standardized processing of net ecosystem exchange measured with eddy covariance technique: algorithms and uncertainty estimation. *Biogeosciences* **3**, 571–583.
- Prioul, J. L. and Chartier, P. 1977. Partitioning of transfer and carboxylation components of intracellular resistance to photosynthesis CO₂ fixation. *Ann. Bot.* **41**, 789–800.
- Reichstein, M., Falge, E., Baldocchi, D., Papale, D., Aubinet, M. and co-authors. 2005. On the separation of net ecosystem exchange into assimilation and ecosystem respiration: review and improved algorithm. *Global Change Biol.* **11**, 1–16.
- Reverter, B. R., Carrara, A., Fernández, A., Gimeno, C., Sanz, M. J. and co-authors. 2011. Adjustment of annual NEE and ET for the open-path IRGA self-heating correction: magnitude and approximation over a range of climate. *Agric. Forest Meteorol.* **151**, 1856–1861.
- Reverter, B. R., Sánchez-Canete, E. P., Resco, V., Serrano-Ortiz, P., Oyónarte, C. and co-authors. 2010. Analyzing the major drivers of NEE in a Mediterranean alpine shrubland. *Biogeosciences* **7**, 2601–2611.
- Richardson, A. D. and Hollinger, D. Y. 2005. Statistical modeling of ecosystem respiration using eddy covariance data: maximum likelihood parameter estimation, and Monte Carlo simulation of model and parameter uncertainty, applied to three simple models. *Agric. Forest Meteorol.* **131**, 191–208.
- Richardson, A. D., Hollinger, D. Y., Burba, G. G., Davis, K. J., Flanagan, L. B. and co-authors. 2006. A multi-site analysis of random error in tower-based measurements of carbon and energy fluxes. *Agric. Forest Meteorol.* **136**, 1–18.
- Saito, M., Miyata, A., Nagai, H. and Yamada, T. 2005. Seasonal variation of carbon dioxide exchange in rice paddy field in Japan. *Agric. Forest Meteorol.* **135**, 93–109.
- Sakai, R. K., Fitzjarrald, D. R. and Moore, K. R. 2001. Importance of low-frequency contributions to eddy fluxes observed over rough surface. *J. Appl. Meteorol.* **40**, 2178–2192.
- Serrano-Ortiz, P., Kowalski, A. S., Domingo, F., Ruiz, B. and Alados-Arboledas, L. 2008. Consequences of uncertainties in CO₂ density for estimating net ecosystem CO₂ exchange by open-path eddy covariance. *Bound. Lay. Meteorol.* **126**, 209–218.
- Takagi, K., Fukuzawa, K., Liang, N., Kayama, M., Nomura, M. and co-authors. 2009. Change in CO₂ balance under a series of forestry activities in a cool-temperate mixed forest with dense undergrowth. *Global Change Biol.* **15**, 1275–1288.
- Takagi, K., Hirata, R., Wen, X., Kwon, H., Saigusa, N. and co-authors. 2008. Inter-comparison of eddy flux calculation and QC/QA procedures of three flux networks (ChinaFLUX, JapanFlux and KoFlux) under AsiaFlux. *AsiaFlux Newsl.* **26**, 8–11.
- Ueyama, M., Harazono, Y., Ohtaki, E. and Miyata, A. 2006. Controlling factors on the inter-annual CO₂ budget at a sub-arctic black spruce forest in interior Alaska. *Tellus* **58B**, 491–501.
- Ueyama, M., Ichii, K., Hirata, R., Takagi, K., Asanuma, J. and co-authors. 2010. Simulating carbon and water cycles of larch forests in East Asia by the BIOME-BGC model with AsiaFlux data. *Biogeosciences* **7**, 959–977.
- Ueyama, M., Hamotani, K., Nishimura, W., Takahashi, Y., Saigusa, N. and co-author. 2012. Continuous measurement of methane flux over a larch forest using a relaxed eddy accumulation method. *Theor. Appl. Climatol.* DOI: 10.1007/s00704-012-0587-0.
- Valentini, R., Matteucci, G., Dolman, A. J., Schulze, E.-D., Rebmann, C. and co-authors. 2000. Respiration as the main determinant of carbon balance in European forests. *Nature* **404**, 861–865.
- Vickers, D. and Mahrt, L. 1997. Quality control and flux sampling problems for tower and aircraft data. *J. Atmos. Oceanic Technol.* **14**, 512–526.
- Webb, E. K., Pearman, G. I. and Leuning, R. 1980. Correction of flux measurements for density effects due to heat and water vapour transfer. *Quart. J. Roy. Meteorol. Soc.* **106**, 85–100.
- Wilczak, J. M., Oncley, S. P. and Stage, S. A. 2001. Sonic anemometer tilt correction algorithms. *Bound.-Lay. Meteorol.* **99**, 127–150.
- Wilson, K., Goldstein, A., Falge, E., Aubinet, M., Baldocchi, D. and co-authors. 2002. Energy balance closure at FLUXNET sites. *Agric. Forest Meteorol.* **113**, 223–243.